CANCER

Successful targeting of PD-1/PD-L1 with chimeric antigen receptor-natural killer cells and nivolumab in a humanized mouse cancer model

Wai Nam Liu[1], Wing Yan So[1], Sarah L. Harden[1], Shin Yie Fong[1], Melissa Xin Yu Wong[1], Wilson Wei Sheng Tan[1], Sue Yee Tan[1], Jessica Kai Lin Ong[1], Ravisankar Rajarethinam[1], Min Liu[1], Jia Ying Cheng[1], Lisda Suteja[2], Joe Poh Sheng Yeong[1], N. Gopalakrishna Iyer[2,3], Darren Wan-Teck Lim[1,4]*, Qingfeng Chen[1,5,6]*

In recent decades, chimeric antigen receptor (CAR)–engineered immune effector cells have demonstrated promising antileukemic activity. Nevertheless, their efficacy remains unsatisfactory on solid cancers, plausibly due to the influence of tumor microenvironments (TME). In a novel mouse cancer model with a humanized immune system, tumor-infiltrating immunosuppressive leukocytes and exhausted programmed death protein-1 (PD-1)^{high} T cells were found, which better mimic patient TME, allowing the screening and assessment of immune therapeutics. Particularly, membrane-bound programmed death ligand 1 (PD-L1) level was elevated on a tumor cell surface, which serves as an attractive target for natural killer (NK) cell–mediated therapy. Hematopoietic stem cell–derived CAR-NK (CAR pNK) cells targeting the PD-L1 showed enhanced in vitro and in vivo anti-solid tumor function. The CAR pNK cells and nivolumab resulted in a synergistic anti-solid tumor response. Together, our study highlights a robust platform to develop and evaluate the antitumor efficacy and safety of previously unexplored therapeutic regimens.

INTRODUCTION

Conventional therapies for patients with cancer include chemotherapy and/or radiotherapy, which lack specificity and are usually accompanied by side effects (*1*). Various innovative approaches, such as targeted therapy and gene therapy, are currently under evaluation (*1*). The early success of immune checkpoint inhibitors (ICI) has revolutionized cancer treatment (*2*), which may partially restore the cytotoxic function of tumor-infiltrating T cells (*3*). For instance, ipilimumab, an anti-cytotoxic T lymphocyte–associated protein 4 (CTLA-4) monoclonal antibody, was the first ICI approved by the Food and Drug Administration (FDA) to treat patients with late-stage melanoma in 2011. Dual therapy using ipilimumab and nivolumab [anti–programmed death protein-1 (PD-1) antibody] was subsequently FDA-approved for the frontline treatment of advanced melanoma in 2015. However, the response rates for most solid tumors are still far from satisfactory, and most patients are refractory to this treatment (*4*). In addition, there are immune-related adverse events (irAE) observed in patients who are treated differently from classical chemotherapy-related toxicity (*5*).

Apart from the ICI, cell-mediated therapy using T cell receptor–engineered T cells and chimeric antigen receptor (CAR)–T cells represents another class of manipulating the immune system to treat patients with cancer (*6*, *7*). To date, more than 500 CAR-T clinical trials have been conducted, and CAR-T cell products, such as Kymriah, Yescarta, Tecartus, and Breyanzi, are available on the market (*8*). Nevertheless, CAR-T cell therapy usually requires gene editing of autologous T cells from patients with cancer, which can be time-consuming and delay emergent treatment (*9*). T cell–mediated therapy is also potentially associated with graft-versus-host disease, cytokine release syndrome (CRS), immune effector cell–associated neurotoxicity syndrome, and cytopenias (*10*, *11*).

Natural killer (NK) cells are capable of killing tumor cells directly by releasing granzyme and perforin or producing interferon-γ (IFN-γ) to mount an adaptive immune response (*12*, *13*). Contrary to T cell–mediated therapy, NK cell–mediated therapy serves as a safer and more effective option for cancer immunotherapy (*14*). NK cell function is independent of human leukocyte antigen matching, thus allowing allogeneic infusion in patients with cancer, and banking "off-the-shelf" CAR-NK cells may reduce time and cost for patients with cancer (*15*). To achieve this purpose, the NK cells can be differentiated from human embryonic stem cells (hESCs) or induced pluripotent stem cells (iPSCs), where these NK cells may be gene-edited to generate target-specific CAR-NK cells (*16*, *17*).

To date, CAR-NK cell–mediated therapy has represented an emerging paradigm for antileukemic treatment, and clinical trials are being conducted globally (*8*). Similar to T cell–mediated therapy, the antitumor efficacy of NK cell–mediated therapy is less optimistic in solid cancers, plausibly due to poor infiltration and exhaustion of effector cells in the tumor inflammatory milieu (*18*, *19*). Tumor microenvironments (TME) consist of tumor cells, endothelial cells, stromal cells, and fibroblasts, with a unique cytokine and chemokine milieu for recruiting and modulating the phenotype of human immune cells, particularly those cells of myeloid lineage (*20*, *21*).

Conventional in vivo models, such as nude mice and nonobese diabetic-severe combined immunodeficiency interleukin-2 (IL-2) receptor gamma chain-null (NSG) mice, lack an immune background that limits the understanding of immunological response during the progression of cancers, as well as the evaluation of antitumor efficacy of treatments, particularly immunotherapy. In addition, immune-related toxicities are mediated by the host immune system after

[1]Institute of Molecular and Cell Biology, Agency for Science, Technology and Research, 138673, Singapore. [2]Duke-NUS Medical School, 169857, Singapore. [3]Department of Head and Neck Surgery, National Cancer Centre Singapore, 169610, Singapore. [4]Division of Medical Oncology, National Cancer Center Singapore, 169610, Singapore. [5]Department of Microbiology and Immunology, Yong Loo Lin School of Medicine, National University of Singapore, 117593, Singapore. [6]Singapore Immunology Network, Agency for Science, Technology and Research, 138648, Singapore.
*Corresponding author. Email: qchen@imcb.a-star.edu.sg (Q.C.); darren.lim.w.t@singhealth.com.sg (D.W.-T.L.)

receiving immune cell therapy (*11*), hence the lack of an in vivo humanized immune system may hamper their assessment. In this regard, our group has recently established a novel humanized mouse nasopharyngeal carcinoma–patient-derived xenografts (NPC-PDX) model for testing immunotherapy (*22*). Similar to primary tumors, tumor-infiltrating lymphocytes (TIL) were found in the NPC-PDX in humanized mice but not in the PDX in NSG mice (*22*, *23*), and pharmacodynamic modulation of the immune checkpoint proteins was observed.

In the present study, we first delineated transcriptomic differences in NPC-PDX between humanized mice and NSG mice. In addition to TIL, human cytokines and chemokines were detected in the tumors from humanized mice. These elements are crucial to remodel TME and better mimic the TME in patients with cancer. In particular, plasma soluble programmed death ligand 1 (sPD-L1) was found in tumor-bearing humanized mice, and membrane-bound PD-L1 was highly expressed in these tumors, thus serving as an excellent target for immune cell therapy. From our results, CAR-expressing NK92 cells and hematopoietic stem cell (HSC)–derived primary NK (CAR pNK) cells targeting PD-L1 could inhibit the growth of different solid cancers that express PD-L1, both in vitro and in vivo, while exhibiting minimal cytotoxicity on primary human hepatocytes (PHH) and side effects in humanized mice. Intriguingly, NPC-PDX showed an increase in the antigen processing and presentation pathway in CAR pNK cell–injected humanized mice. Because tumor-infiltrating T cells displayed exhaustion phenotypes, combination therapy involving the CAR pNK cells and nivolumab was applied to the mice, which resulted in a synergistic anti-solid tumor response, suggesting that restoration of T cell function by specific ICI could further inhibit the growth of tumors after sensitization by the NK cell–mediated therapy.

In summary, HSC-derived CAR pNK cells highlight a potential off-the-shelf therapeutic option for patients with solid cancers. By combining NK cell–mediated therapy and ICI therapy, we demonstrated better antitumor efficacy in our humanized mouse NPC-PDX model. As other exhaustion markers, such as T cell immunoreceptor with immunoglobulin (Ig) and ITIM domains (TIGIT) and T cell Ig and mucin-domain containing-3 (TIM-3) were up-regulated in the tumor-infiltrating T cells and NK cells, other combination regimens can be assessed using this robust preclinical platform. This will enable preclinical evaluation of previously unexplored therapeutic strategies to treat cancers and may potentially predict and improve patients' clinical outcomes.

RESULTS

The presence of a humanized immune system changes the profile of TME

TIL play a pivotal role to shape TME and influence clinical outcomes of cancer treatments (*24*). Therefore, our mouse cancer model with a humanized immune system serves as a better platform to screen for potential biomarkers and evaluate the efficacy of therapeutics when compared to traditional immunocompromised mouse cancer model (*22*). To gain insights into the transcriptomic and proteomic difference of the tumors, NPC-PDX were engrafted in NSG mice and humanized mice. Four weeks after the transplant, the tumors were harvested and subjected to RNA sequencing, and their sequencing data were compared (Fig. 1A). Heatmap analysis of differentially expressed (DE) genes demonstrated that their transcriptomic profile was distinct (Fig. 1B), indicating that the PDX was greatly influenced by the infiltration of $CD45^+$ humanized immune cells (fig. S1A). Several molecular pathways, including T cell receptor (*PTPRC*, *ICOS*, and *CD3E*), cytokine-related (*IL2RB*, *CCR5*, and *CD40LG*), and chemokine-related signaling (*ITK*, *CCR5*, and *PIK3CG*) were significantly up-regulated in the tumors from humanized mice (Fig. 1C). Proteomic analysis further revealed that the expressions of C-X-C motif chemokine ligand 10 (CXCL10), IL-8, and plasminogen activator inhibitor-1 (PAI-1) were augmented in the tumors from humanized mice (Fig. 1D), which are known to be positively correlated with the recruitment of regulatory T cells (*25*, *26*), myeloid-derived suppressor cells (MDSC), and M2 macrophages (*27*–*29*). Notably, the CXCL10 could also promote the recruitment of $CD8^+$ T cells in the tumors (*30*). Flow cytometry analysis confirmed that $CD8^+$ T cells ($hCD45^+hCD3^+hCD8^+$), regulatory T cells ($hCD45^+hCD3^+hCD4^+hCD25^+hCD127^{low}$), and two subsets of MDSC, including polymorphonuclear (PMN)–MDSC ($hCD45^+hCD11b^+hCD33^+hHLA\text{-}DR^-hCD14^-hCD15^+$) and early-stage (E)–MDSC ($hCD45^+hCD11b^+hCD33^+hHLA\text{-}DR^-hCD14^-hCD15^-$), infiltrated the tumors in humanized mice but not in NSG mice (fig. S1, B to D). Apart from local immune responses in the TME, various inflammatory cytokines (IFN-γ, IL-8, and IL-18), chemokine (MCP-1), and immune checkpoint biomarkers [Galectin-9 (Gal-9), sPD-L1, sCD25, and transforming growth factor–β1 (TGF-β1)] were found in the periphery of PDX-bearing humanized mice, while these soluble mediators were minimally detected in NSG mice (fig. S2).

From the RNA sequencing data, it was shown that gene expression levels of several exhaustion markers, including *CTLA4* and *PDCD1*, were highly up-regulated in the NPC-PDX from humanized mice (Fig. 1E). By flow cytometry, it was validated that the expression of PD-1 was more pronounced in tumor-infiltrating $CD8^+$ T cells and $CD56^+$ NK cells ($hCD45^+hCD3^-hCD16^+hCD56^+$) than those in circulating $CD8^+$ T cells and $CD56^+$ NK cells (Fig. 1, F and G). Intriguingly, other exhaustion markers, such as TIGIT and TIM-3, were consistently up-regulated in the T cells and NK cells in the PDX (fig. S3). As revealed by multiplex immunohistochemical images obtained from paired archival tissue of the donor patients, $CD8^+$ T cells and $FOXP3^+$ regulatory T cells were found, and these cells expressed PD-1 and/or CTLA-4 in the primary NPC tumors (fig. S4), suggesting that the composition of immune cell infiltration is comparable between PDX and primary tumors.

As sPD-L1 was found in circulation, we also examined its membrane-bound expression level in the tumors from NSG mice and humanized mice. It was found that transcriptional and surface protein levels of PD-L1 were significantly higher in the isolated tumor cells from humanized mice (Fig. 1, H and I). This result was validated by in situ immunohistochemistry staining of PD-L1 in tumors (Fig. 1J). Notably, some of the tumor-infiltrating $CD45^+$ immune cells expressed PD-L1 (fig. S5), and it has been suggested that other nonimmune epithelial cells and stromal cells could also express the PD-L1 (*31*, *32*). The increment in the expression level of PD-L1 possibly results in T cell and NK cell exhaustion in the tumors via PD-1/PD-L1 axis (*33*, *34*), which have been targeted by respective ICI, such as anti–PD-1 or anti–PD-L1 monoclonal antibodies. We further explored the possibility of using cell-mediated therapy to target the elevated PD-L1 expressed on solid tumor cell surface.

CAR-engineered NK92 cells enhance the killing of PD-L1–expressing cancers

Third-generation CAR technology was applied in this study to generate NK cells targeting PD-L1, which consists of an anti–PD-L1

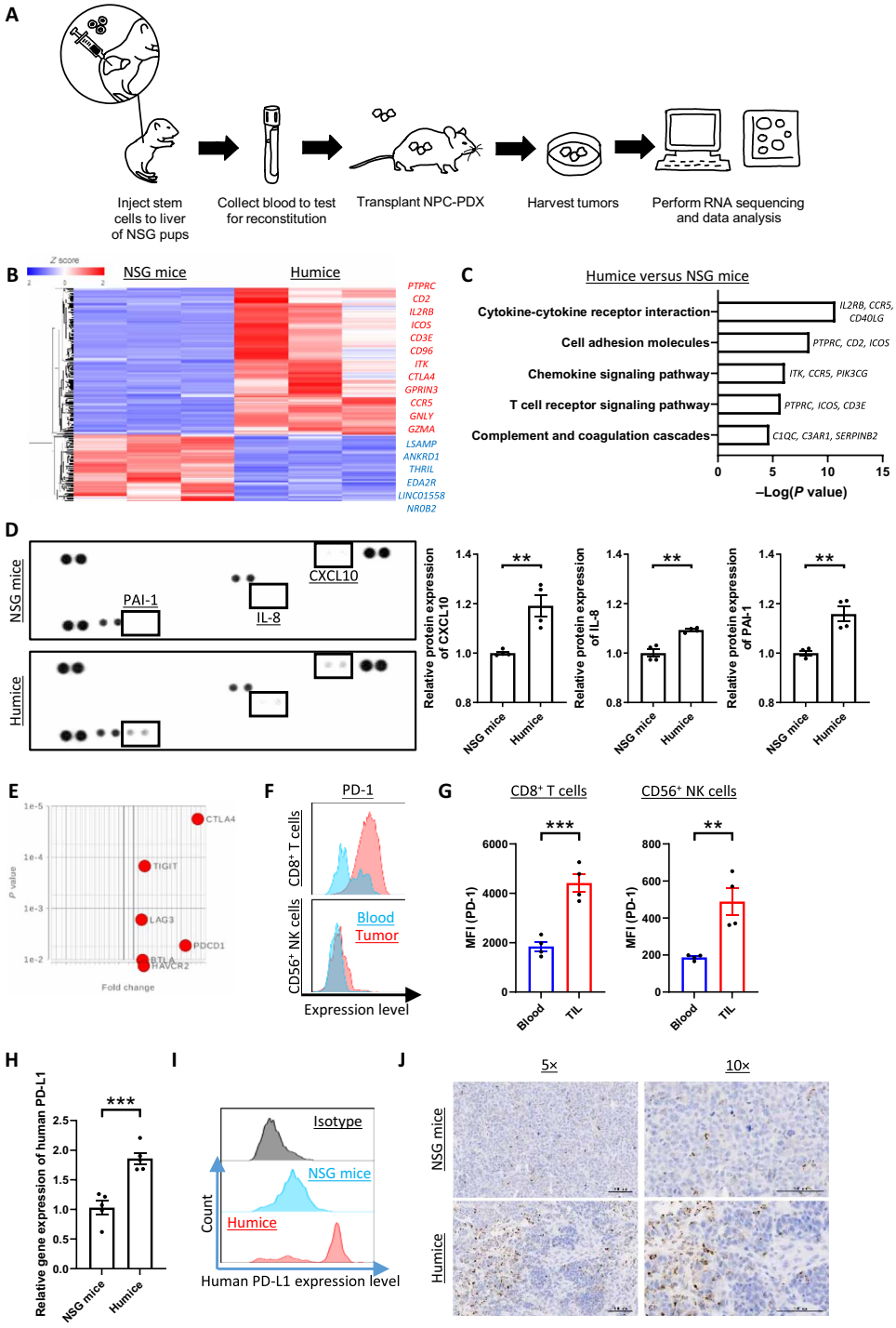

Fig. 1. TME in humanized mice is distinct from that in immunocompromised NSG mice. (**A**) Schematic description showing the methodology to generate humanized mice and workflow for RNA sequencing using NPC-PDX from humanized mice and NSG mice. (**B**) Heatmap of DE genes from NPC-PDX between humanized mice ($n = 3$) and NSG mice ($n = 3$) is shown. (**C**) Signaling pathway analysis of DE genes. (**D**) Relative protein expressions of CXCL-10, IL-8, and PAI-1 in tumor lysate from NSG mice ($n = 4$) and humanized mice ($n = 4$). Data are expressed as means ± SEM. $^{**}P < 0.01$, two-tailed unpaired t test. (**E**) Volcano plot of selected DE genes between humanized mice and NSG mice is shown. (**F** and **G**) Surface expressions of PD-1 on $CD3^+CD8^+$ T cells and $CD3^-CD16^+CD56^+$ NK cells in circulation (blue histogram) and in tumor (red histogram) were analyzed by flow cytometry. Data are expressed as means ± SEM. $^{**}P < 0.01$ and $^{***}P < 0.001$, two-tailed unpaired t test ($n = 4$ for both groups). MFI, mean fluorescence intensity. (**H**) Relative mRNA expression level of human PD-L1 on tumor cells isolated from NPC-PDX from NSG mice ($n = 5$) and humanized mice ($n = 5$). Data are expressed as means ± SEM. $^{***}P < 0.001$, two-tailed unpaired t test. (**I**) Surface expression of human PD-L1 on tumor cells. Isotype control (black histogram), cells harvested from NSG mice (blue histogram), and humanized mice (red histogram) were analyzed by flow cytometry. (**J**) Representative photomicrographs showing immunohistochemical staining of human PD-L1 on NPC-PDX from NSG mice and humanized mice. Scale bars, 100 μm. $n = 3$ per group.

single-chain fragment variable (ScFv), a spleen focus-forming virus promoter to enhance the gene expression level, a CD8 hinge (H) and transmembrane (TM) domain, two costimulatory domains (CD28 and 4-1BB), and a CD3ζ activation domain. In addition, an endogenous green fluorescence protein (eGFP) reporter gene was inserted, and a puromycin resistance gene allowed us to establish a stable CAR NK92 cell line for robust validation of its antitumor efficacy, both in vitro and in vivo (Fig. 2A). Successful transduction was demonstrated by immunofluorescence staining (fig. S6A), and expression of CAR on the NK92 cell surface was further confirmed by flow cytometry (fig. S6B). In the absence of IFN-γ, HepG2 cells expressed a lower level of PD-L1 on their cell surface (Fig. 2B), and the cytotoxicity of CAR NK92 cells on untreated HepG2 cells was minimal (Fig. 2C). Pretreatment of the HepG2 cells with IFN-γ induced PD-L1 expression, and the killing ability of CAR NK92 cells on the IFN-γ–treated cells was increased drastically (Fig. 2, B and C). In addition, various human cancer cell lines, including A549, C666-1, and Panc 08.13 cells that constitutively expressed the PD-L1, were cocultured with the CAR NK92 cells (Fig. 2B). Our results demonstrated that the CAR NK92 cells were able to lyse their target cells more effectively when compared to those nontransduced wild-type (WT) NK92 cells (Fig. 2C), suggesting that our CAR-NK cells can target a broad spectrum of cancer types as long as they express PD-L1. Apart from direct killing, NK cells are also known to lyse their target cells through apoptosis (*35*). Without prior stimulation of the IFN-γ, there were no significant changes in the apoptotic rate in the HepG2 cells (Fig. 2D). In contrast, the CAR NK92 cells could induce apoptosis in the IFN-γ–treated HepG2 cells and other human cancer cells (Fig. 2D), accompanied by an increase in NK cell CD107a expression, which indicates a release of cytotoxic granule (Fig. 2E). By enzyme-linked immunosorbent assay (ELISA), it was further revealed that IFN-γ was secreted from the CAR NK92 cells upon stimulation with those PD-L1–expressing cancer cells (Fig. 2F).

To evaluate in vivo anti-solid tumor efficacy of CAR NK92 cells, C666-1 cells, and NPC-PDX were inoculated into NSG mice. Upon the formation of visible tumors, which took approximately 1 to 2 weeks, the mice received scheduled NK cell–mediated therapy (Fig. 3A). Compared to saline-injected and WT NK92 cell–injected mice, the tumor size and weight of C666-1 were diminished in the CAR NK92 cell–treated group (Fig. 3, B to D). Similarly, the in vivo antitumor effect of CAR NK92 cells was demonstrated on the PD-L1–expressing NPC-PDX (Fig. 3, E to G), where the PDX were established from primary tumors of three patients. Apart from the NPC, it was found that the CAR NK92 cells could also exhibit growth inhibitory effects on PD-L1–expressing A549 tumors (fig. S7, A to D) and lung adenocarcinoma (LAC)–PDX, respectively, in the NSG mice (fig. S7, A and E to G). These results demonstrated that the CAR-NK cells are efficient in killing various solid cancer types, both in vitro and in vivo.

HSC-derived primary CAR-NK cells are efficient in killing PD-L1–expressing solid cancers

Before infusing cells of malignant origin into patients, NK92 cells need to be irradiated to avoid in vivo proliferation (*36*). To minimize safety concerns, primary NK cells are preferably used for CAR-NK cell–mediated therapy in clinics (*37*). In recent years, it has been demonstrated that hESCs and iPSCs could be differentiated into NK cells, which showed similar phenotypes and functions to those mature NK cells in peripheral blood (*38*, *39*). In the present study, $CD34^+$ HSC in human umbilical cord blood were expanded and differentiated into primary NK (pNK) cells in a feeder cell-free system (fig. S8, A and B). By flow cytometric analysis, it was found that the phenotype of HSC-derived pNK cells was similar to that of cord blood NK (CB-NK) cells (Fig. 4A), despite the expression level of CD16 of the latter being higher. In terms of their functions, CB-NK cells and pNK cells exhibited similar cytotoxicity toward K-562 cells (Fig. 4B) and induced apoptosis of the K-562 cells (Fig. 4C). In addition, their expression levels of CD107a and release of IFN-γ were comparable after the coculture (Fig. 4, D and E). Next, CAR pNK cells were generated by lentiviral transduction. The efficiency varied from 20 to 40%, subject to batch-to-batch variation of the stem cells (fig. S8, C and D). Notably, the transduction was more efficient than infecting the CB-NK cells directly (fig. S8D), thus resulting in a much higher yield of the CAR pNK cells. Apart from killing C666-1 cells, the CAR pNK cells could also lyse tumor cells isolated from the NPC-PDX (Fig. 4F) and trigger apoptosis in the tumor cells by increasing the NK cell CD107a expression and IFN-γ release (Fig. 4, G to I). In addition, the CAR pNK cells were capable of killing other PD-L1–expressing cancer cell lines (fig. S8E).

In vivo function of the CAR pNK cells were then assessed alongside nontransduced pNK (WT pNK) cells and CAR-expressing primary T (CAR pT) cells to compare their antitumor efficacy, following the treatment schedule as shown in Fig. 3A. A reduction of tumor burden was observed in NSG mice treated with the CAR pNK cells, but not the CAR pT cells, suggesting that the former displayed a higher antitumor potency in our NPC-PDX model (Fig. 5, A to C). The tumors were harvested 2 days after the last cell-mediated therapy. Fluorescence-activated cell sorting (FACS) analysis and histological examinations revealed the presence of tumor-infiltrating NK cells and T cells (Fig. 5, D to F). Despite a greater number of CAR pT cells persisting in the PDX, the results from terminal deoxynucleotidyl transferase–mediated deoxyuridine triphosphate nick end labeling (TUNEL) illustrated that more tumor cells underwent apoptosis after the injection of CAR pNK cells (Fig. 5, G and H).

As mentioned earlier, the immunosuppressive TME in humanized mouse model was found to more closely resemble that in patients as compared to NSG mice. Therefore, we further assessed the efficacy and immunotoxicity of CAR-NK cell–mediated therapy in humanized mice transplanted with NPC-PDX (Fig. 6A). After the injection of CAR pNK cells and CAR pT cells, there was an increase in the plasma IFN-γ level, and the elevation was more pronounced in the CAR pT cell–treated mice (fig. S9A). Because the expression level of PD-L1 could be induced by IFN-γ in vitro, we further examined the modulation of the plasma sPD-L1 level in the mice. Accompanied by the increase in IFN-γ levels, the sPD-L1 levels in circulation were increased in both groups, particularly in the CAR pT cell–treated mice (fig. S9B). To demonstrate that there were no premature death of the CAR pNK cells and CAR pT cells in circulation, these cells were treated with human sPD-L1 recombinant protein in vitro. Our results showed that there were no significant changes in their viability (fig. S9C) while increasing their release of IFN-γ (fig. S9D), suggesting that these cells might also be activated in the circulation after binding to the sPD-L1 before reaching the tumor sites in humanized mice. Apart from the plasma IFN-γ and sPD-L1, it was also found that the transcriptome expression levels of IFN-γ and PD-L1 were augmented more drastically in the PDX after the CAR pT cell therapy (fig. S9, E and F). Intriguingly, tumor burden was reduced after the mice were injected with the CAR pNK cells (Fig. 6, B to D)

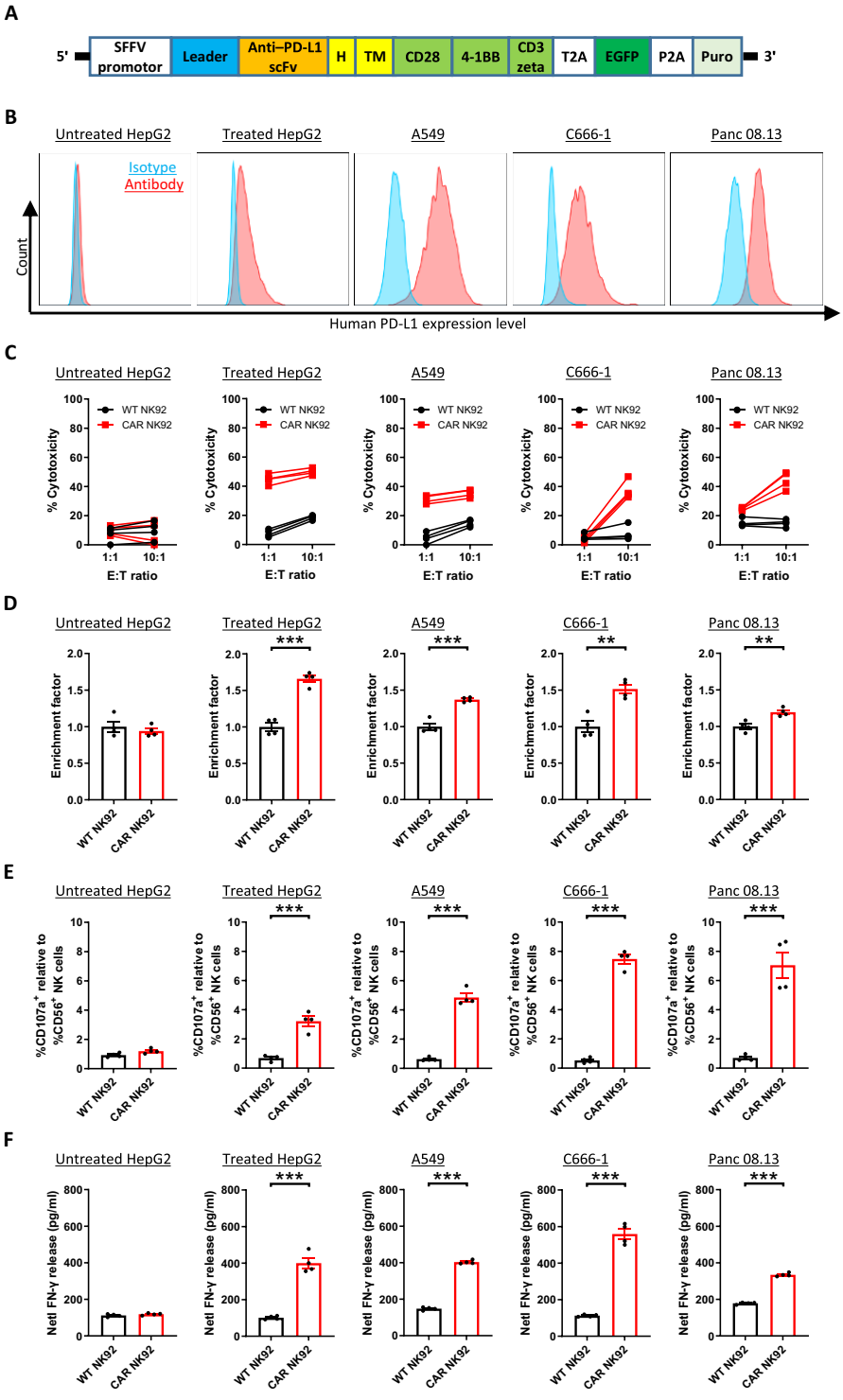

Fig. 2. Enhanced in vitro antitumor activity in CAR-expressing NK92 cells. (**A**) Design of CAR construct. Puro, puromycin. SFFV, spleen focus-forming virus. (**B**) Surface expression of human PD-L1 on HepG2 (untreated or IFN-γ–treated), A549, C666-1, and Panc 08.13 cells. Cells stained with isotype control (blue histogram) and anti–PD-L1 antibody (red histogram) were examined by flow cytometry. WT NK92 cells ($n = 4$) and CAR NK92 cells ($n = 4$) were cocultured with various human cancer cell lines at the indicated E:T ratios (**C**) or at a 10:1 ratio of E:T (**D** to **F**). (C) The percentages of NK cell cytotoxicity on different cancer cell lines are shown. (D) The extent of apoptosis as indicated by enrichment factor. (E) CD107a expression was determined in anti-CD56–labeled NK cells after stimulation by different cancer cell lines. (F) Net release of IFN-γ after stimulation by different cancer cell lines. Data from (D) to (F) are expressed as means ± SEM. $^{**}P < 0.01$ and $^{***}P < 0.001$, two-tailed unpaired *t* test.

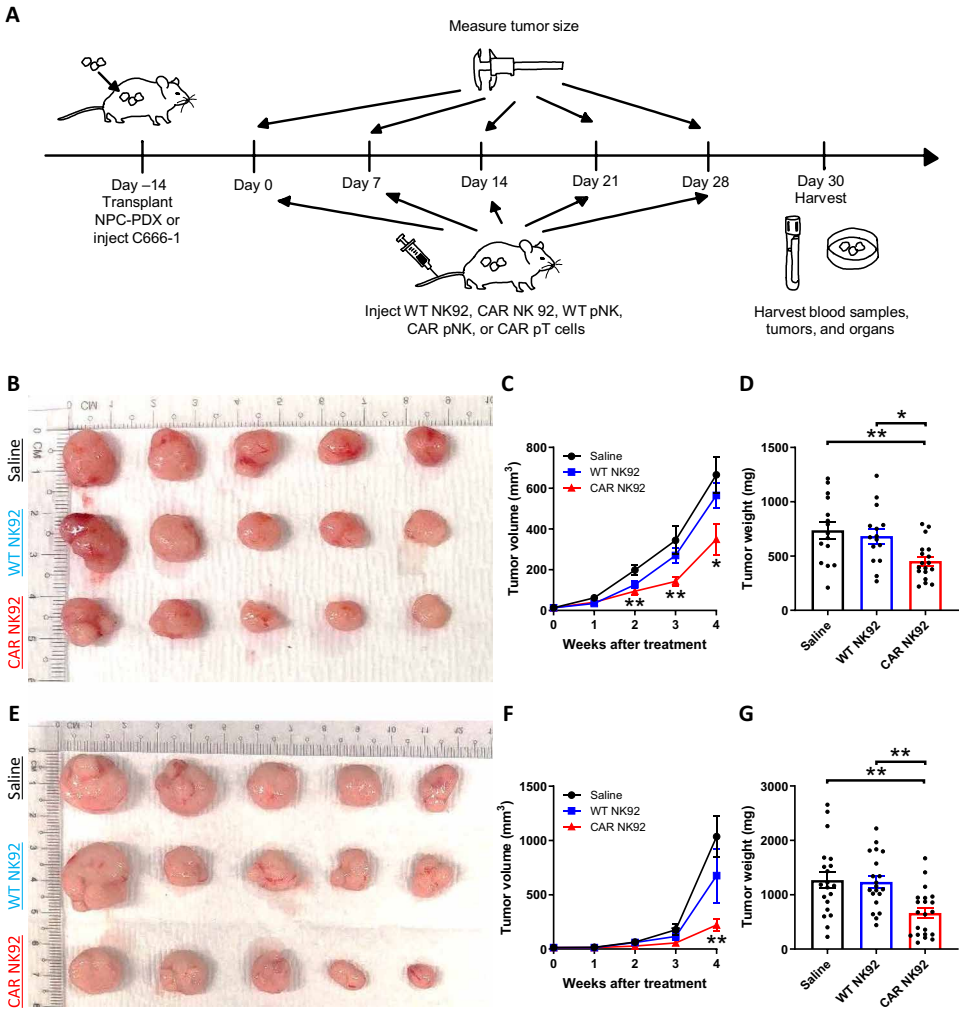

Fig. 3. CAR-expressing NK92 cells exhibit better anti-solid tumor effect in NSG mice. (**A**) Schematic description of tumor inoculation and cell-mediated therapy in NSG mice. The mice were either injected with C666-1 cells or transplanted with NPC-PDX, which usually took 1 to 2 weeks to form visible tumors. (**B** to **D**) NSG mice were inoculated with C666-1 cells. After the formation of visible tumors, the mice were injected with saline ($n = 15$), WT NK92 cells ($n = 15$), and CAR NK92 cells ($n = 18$). (B) Representative image of tumors. (C) Tumor volumes are shown. Data are expressed as means ± SEM. $^{*}P < 0.05$ and $^{**}P < 0.01$, one-way analysis of variance (ANOVA) followed by multiple comparisons, when CAR NK92 cell–injected group is compared to saline-injected group. (D) Tumor weights are shown. Data are combined from two independent experiments and expressed as means ± SEM. $^{*}P < 0.05$ and $^{**}P < 0.01$, one-way ANOVA followed by multiple comparisons. (**E** to **G**) NSG mice were transplanted with NPC-PDX. After the formation of visible tumors, the mice were injected with saline ($n = 20$), WT NK92 cells ($n = 20$), and CAR NK92 cells ($n = 21$). (E) Representative image of tumors. (F) Tumor volumes are shown. Data are expressed as means ± SEM. $^{**}P < 0.01$, one-way ANOVA followed by multiple comparisons, when CAR NK92 cell–injected group is compared to saline-injected group. (G) Tumor weights are shown. Data are combined from three independent experiments using PDX derived from three patients and expressed as means ± SEM. $^{**}P < 0.01$, one-way ANOVA followed by multiple comparisons.

despite the presence of tumor-infiltrating regulatory T cells and MDSC and the influence of the immunosuppressive niche. Nevertheless, mice injected with CAR pT cells did not show significant reduction in tumor weight when compared to the saline control group. Minimal CAR pNK cells and CAR pT cells persisted in the PDX 2 days after the last injection (fig. S10). Of equal importance, the in vitro and in vivo safety of CAR pNK cells was evaluated. As shown in fig. S11A, there was a subtle increase in PD-L1 expression after PHH were treated with IFN-γ, similar to the observation in HepG2 cells (Fig. 2B). Nevertheless, the CAR pNK cells showed a limited increase in cytotoxicity, if any, on the IFN-γ–treated PHH in vitro (fig. S11B), while IFN-γ–treated HepG2 cells were more susceptible to the CAR pNK cells (fig. S8E). By immunofluorescence staining, it was found that some of the tumor-infiltrating $CD45^{+}$ immune cells expressed PD-L1 (fig. S5). Nonetheless, the CAR pNK cells showed minimal increase in cytotoxicity when they were cocultured with the TIL, possibly due to the low expression level of PD-L1 on the immune cells (fig. S11, C and D). Besides, the CAR pNK cells only exhibited mild cytotoxicity on the nonimmune stromal cells while showing better killing effects on the tumor cells (fig. S11, C and D). Recently, it has been reported that the amino acid sequence between human PD-L1 and mouse PD-L1 is well conserved, and their structures are almost identical (*40*). By flow cytometry, we proved that mouse PD-L1 recombinant protein could bind with our CAR (fig. S12A). As shown in fig. S12 (B and C), the mouse PD-L1 expression level in liver and lung was up-regulated

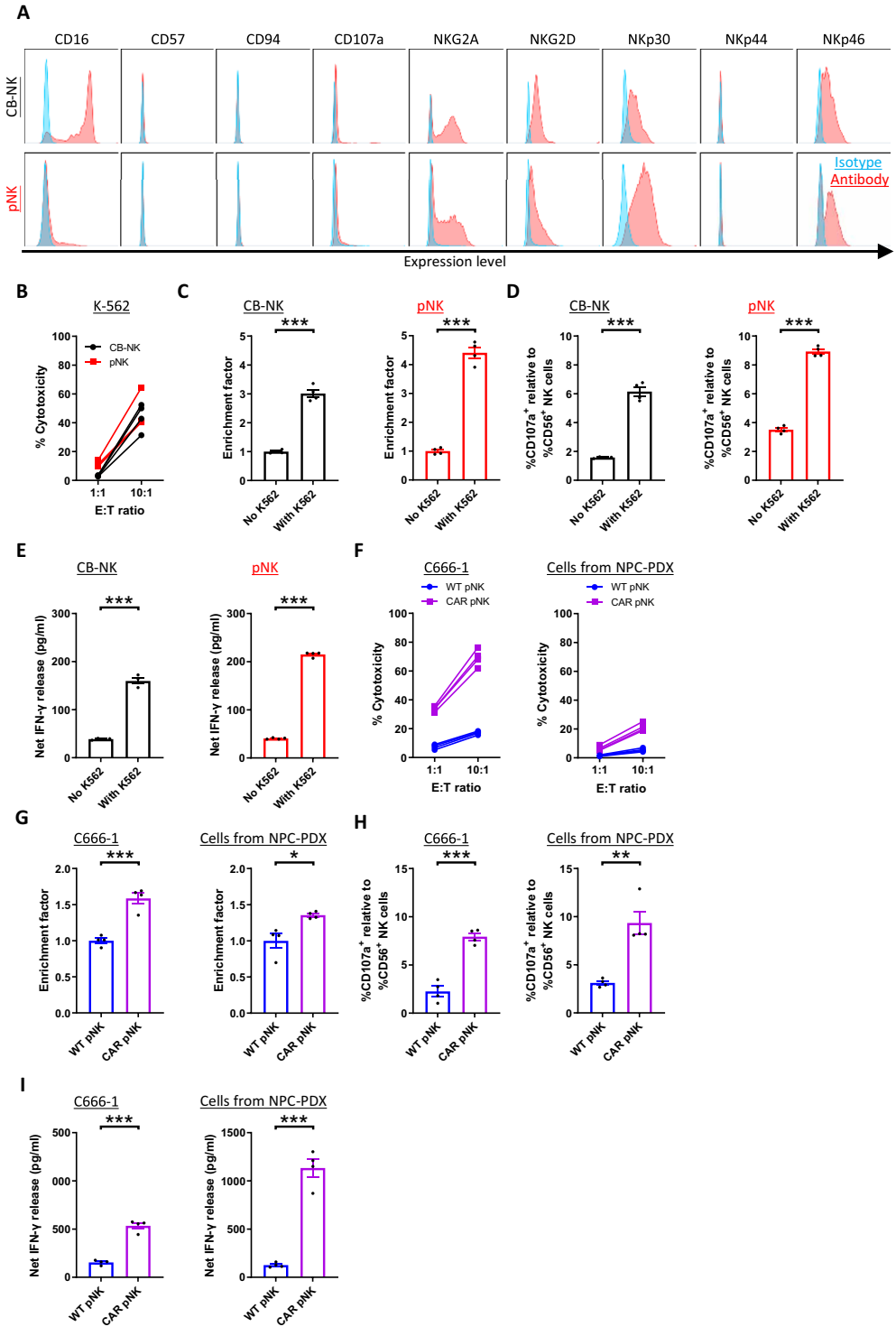

Fig. 4. Phenotypic and functional characterization of CAR-expressing HSC-derived NK cells. (**A**) Surface expressions of NK cell–specific markers under the gate of human CD45$^+$ and CD56$^+$ subset. Cells stained with isotype control (blue histogram) and indicated PE-conjugated antibodies (red histogram) were examined by flow cytometry. CB-NK cells ($n = 4$) and pNK cells ($n = 4$) were cocultured with K-562 cells at the indicated E:T ratios (**B**) or at a 10:1 ratio of E:T (**C** to **E**). (B) The percentages of NK cell cytotoxicity on K-562 cells are shown. (C) The extent of apoptosis as indicated by enrichment factor. (D) CD107a expression was determined in anti-CD56–labeled NK cells after stimulation by K-562 cells. (E) Net release of IFN-γ after stimulation by K-562 cells. WT pNK cells ($n = 4$) and CAR pNK cells ($n = 4$) were cocultured with C666-1 cells or tumor cells isolated from NPC-PDX at the indicated E:T ratios (**F**) or at a 10:1 ratio of E:T (**G** to **I**). (F) The percentages of NK cell cytotoxicity on tumor cells are shown. (G) The extent of apoptosis. (H) CD107a expression on NK cells after stimulation by tumor cells. (I) Net release of IFN-γ after stimulation by tumor cells. Data from (C) to (E) and (G) to (I) are expressed as means ± SEM. *$P < 0.05$, **$P < 0.01$, and ***$P < 0.001$, two-tailed unpaired t test.

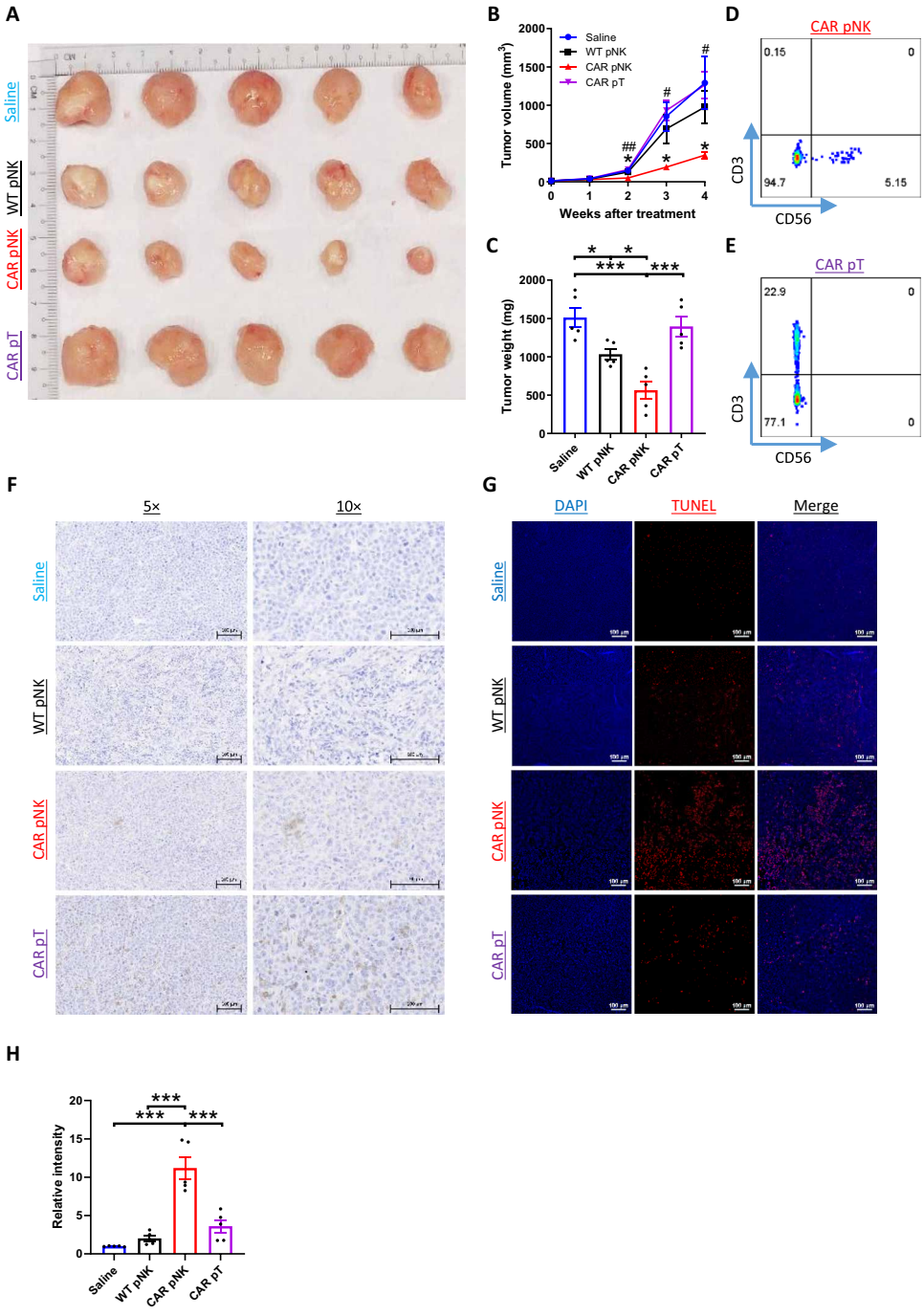

Fig. 5. CAR-expressing primary NK cells suppress in vivo growth of NPC-PDX more effectively. NSG mice were transplanted with NPC-PDX. After the formation of visible tumors, the mice were injected with saline ($n = 5$), WT pNK cells ($n = 5$), CAR pNK cells ($n = 5$), and CAR pT cells ($n = 5$). (**A**) Representative image of tumors. (**B**) Tumor volumes are shown. Data are expressed as means ± SEM, and comparative statistical analysis were done by one-way ANOVA followed by multiple comparisons. *$P < 0.05$, when CAR pNK cell–injected group is compared to saline-injected group; #$P < 0.05$ and ##$P < 0.01$, when CAR pNK cell–injected group is compared to CAR pT cell–injected group. (**C**) Tumor weights are shown. Data are expressed as means ± SEM. *$P < 0.05$ and ***$P < 0.001$, one-way ANOVA followed by multiple comparisons. (**D** and **E**) Representative FACS plots showing the infiltration of $CD3^-CD56^+$ NK cells (D) and $CD3^+CD56^-$ T cells (E) in tumors. (**F**) Representative photomicrographs showing immunohistochemical staining in tumors. The presence of NK and T cells was indicated by the expression of NCR1 and CD3, respectively. Scale bars, 100 μm. $n = 5$ per group. (**G**) Representative photomicrographs showing TUNEL in tumors. Apoptotic cells were labeled by red fluorescence. Scale bars, 100 μm. $n = 5$ per group. DAPI, 4′,6-diamidino-2-phenylindole. (**H**) Signal intensity of TUNEL is quantified from the images, and data are expressed as means ± SEM. ***$P < 0.001$, one-way ANOVA followed by multiple comparisons.

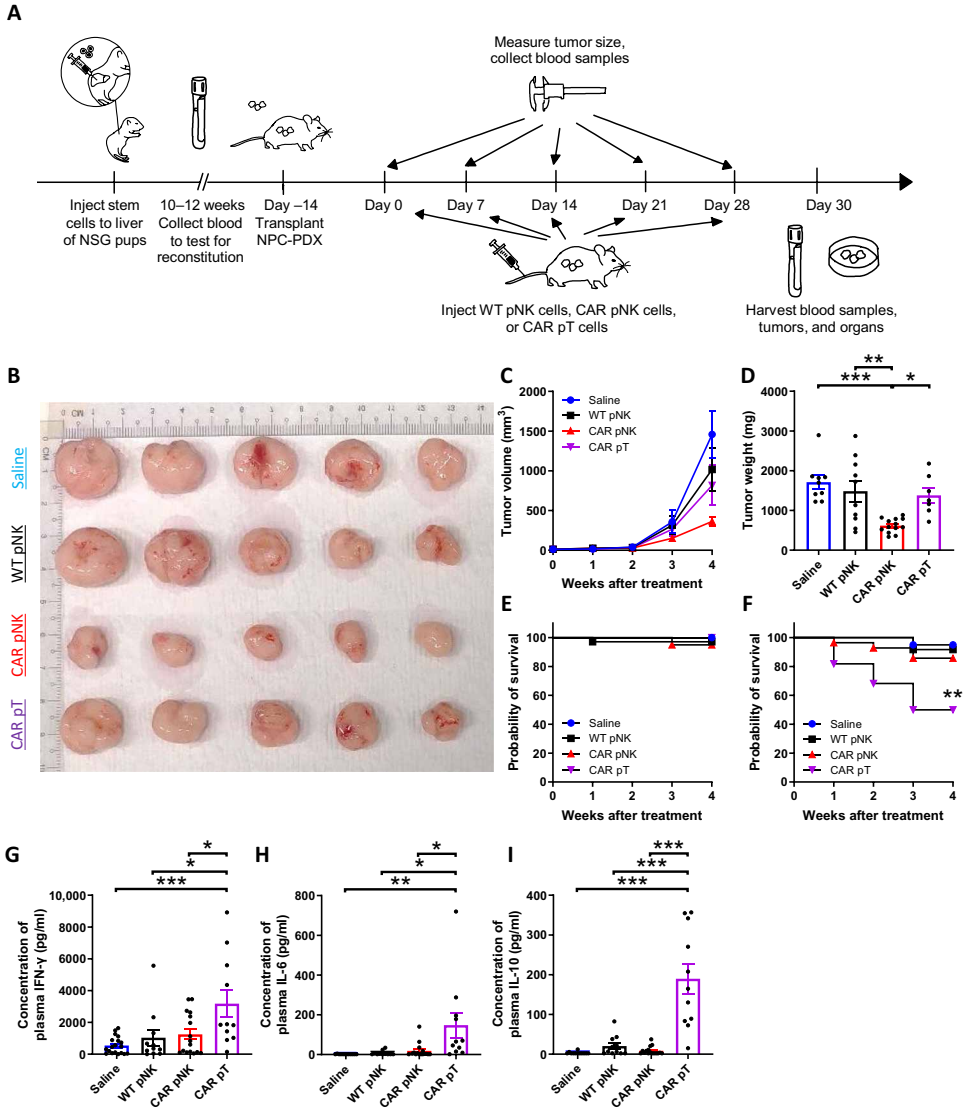

Fig. 6. Evaluation of antitumor efficacy and safety of CAR pNK cells in NPC-PDX–bearing humanized mice. (**A**) Schematic description of PDX engraftment and cell-mediated therapy in humanized mice. (**B** to **D**) Humanized mice were transplanted with NPC-PDX. After the formation of visible tumors, the mice were injected with saline ($n = 9$), WT pNK cells ($n = 10$), CAR pNK cells ($n = 13$), and CAR pT cells ($n = 7$). (B) Representative image of tumors. (C) Tumor volumes are shown. Data are expressed as means ± SEM. (D) Tumor weights are shown. Data are expressed as means ± SEM. *$P < 0.05$, **$P < 0.01$, and ***$P < 0.001$, one-way ANOVA followed by multiple comparisons. (**E**) Survival curve of NSG mice after treatment with saline ($n = 36$), WT pNK cells ($n = 34$), CAR pNK cells ($n = 38$), and CAR pT cells ($n = 20$). Data are combined from at least three independent experiments. (**F**) Survival curve of humanized mice after treatment with saline ($n = 20$), WT pNK cells ($n = 12$), CAR pNK cells ($n = 28$), and CAR pT cells ($n = 22$). Data are combined from at least three independent experiments. The survival rate of mice between CAR pNK cell–injected group and CAR pT cell–injected group is compared by Kaplan-Meier analysis via a log-rank test. **$P < 0.01$. (**G** to **I**) Blood samples were collected from humanized mice 2 days after the last treatment with saline ($n = 12$ for IL-6 and IL-10; $n = 19$ for IFN-γ), WT pNK cells ($n = 11$), CAR pNK cells ($n = 16$), and CAR pT cells ($n = 11$). Plasma concentrations of IFN-γ (G), IL-6 (H), and IL-10 (I) were determined by LEGENDplex. Data are expressed as means ± SEM. *$P < 0.05$, **$P < 0.01$, and ***$P < 0.001$, one-way ANOVA followed by multiple comparisons.

after PDX-bearing humanized mice were treated with CAR pNK cells and CAR pT cells. These cells might also bind to the mouse PD-L1–expressing normal cells in the organs. Intriguingly, the survival rate of NSG mice among different treatment groups was comparable, while a significant reduction in the survival rate was observed in the CAR pT cell–injected humanized mice (Fig. 6, E and F) but not in the CAR pNK cell–treated group. Hence, the decrease in survivability of the CAR pT cell–treated mice might also be contributed by the release of soluble mediators. By LEGENDplex, it was found that plasma concentrations of IFN-γ, IL-6, and IL-10 were significantly elevated in the humanized mice treated with the CAR pT cells but not CAR pNK cells (Fig. 6, G to I). This suggested that the former might elicit CRS in the presence of the humanized immune system. To confirm whether the T cell–mediated therapy led to organ damage, liver and lungs were subjected to pathological evaluation. From the results, the liver and lungs from saline (fig. S13, A and E) and CAR pNK cell–treated groups (fig. S13, B and F) showed normal histology. However, after the treatment of CAR pT cells, there were widespread multifocal aggregates of mononuclear cells that include lymphocytes or histiocytes present in hepatic parenchyma. The mononuclear cells

were mostly confined to perivascular area, and their presence was associated with multinucleated giant cells exhibiting a granulomatous inflammation (fig. S13, C and D). Besides, alveoli were mildly hyperplastic and infiltrated with the moderate presence of mixed inflammatory cells, such as mononuclear cells and, to some extent, few PMN cells in the lungs (fig. S13, G and H). Together, the surge of various cytokines under circulation and pathological conditions in the liver and lung might lead to the reduction in mouse body weight (fig. S13I) and survivability after CAR pT cell–mediated therapy.

Combination therapy using CAR pNK cells and nivolumab shows a synergistic antitumor response in a humanized mouse NPC-PDX model

To investigate the transcriptomic changes in NPC-PDX after cell-mediated therapy and identify potential combination regimens, the tumors were sent for bulk RNA sequencing. Compared to saline-injected group, there was an up-regulation of NK cell–mediated cytotoxicity pathway (*TYROBP*, *KLRD1*, and *FCER1G*), as well as antigen processing and presentation pathway (*CTSL*, *KLRD1*, and *CD8A*) after CAR pNK treatment (Fig. 7, A and B). Because T cells were the predominant immune cell type in the tumors (fig. S1B), we postulated that the presented antigens might be recognized by the tumor-infiltrating T cells for further antitumor effect. Nonetheless, these T cells exhibited exhaustion phenotypes (Fig. 1, F and G), which might impede their functions. To overcome this issue and assay the effect of combination therapy with different ICI, ipilimumab or nivolumab was used along with CAR pNK to block the immune inhibitory signals in TME (Fig. 7C). In line with our previous findings (*22*) and paired outcomes from donor patients treated with immunotherapy (fig. S14), treatments involving these antibodies alone did not reduce the tumor burden of NPC-PDX in humanized mice (Fig. 7, D, F, and G). However, it was found that more $CD3^+$ T cells were present in the PDX when the mice were treated with ipilimumab, and a reduction in CD4/CD8 ratio was observed when the mice received nivolumab treatment (fig. S15). Next, the CAR pNK cells were administered into the mice, in combination with the ICI (Fig. 7C). From our results, the combination of NK cell–mediated therapy and ipilimumab did not further reduce the PDX burden. In contrast, dual therapy using the CAR pNK cells and nivolumab resulted in a synergistic antitumor response in vivo (Fig. 7, E to G), which might partially due to the restoration of host T cell function. Collectively, the NK cell–mediated therapy could sensitize the tumors, increase antigen processing and presentation, and enhance the killing ability of tumor-infiltrating immune cells after the treatment of specific ICI.

DISCUSSION

Cancer immunotherapy using genetically modified immune effector cells represents an emerging treatment option for patients. In particular, CAR expression on NK cells facilitates the recognition of tumor-associated antigens, thus enhancing NK cell cytotoxicity on tumor cells (*8*). Despite their astonishing activity in the treatment of hematological malignancies, the antitumor efficacy remains unsatisfactory in solid cancers (*18*, *19*), likely due to the unique immunosuppressive TME. In the presence of a humanized immune system, our model better simulates the TME in patients when compared to immunocompromised NSG mice (*22*). Hence, we aimed to screen for potential targets for solid cancer treatments based on the TME difference between NSG mice and humanized mice. Our RNA sequencing data revealed that the transcriptomic profile of NPC-PDX in humanized mice is distinct from that in NSG mice, suggesting that the PDX is influenced by the infiltration of $CD45^+$ humanized immune cells, which is congruent with findings from other studies (*41*, *42*). Besides, protein expressions of CXCL-10, IL-8, and PAI-1 were found to be increased in PDX lysate. These mediators are responsible for recruiting tumor-infiltrating regulatory T cells (*25*, *26*) and MDSC (*27*, *28*). Immunosuppressive cell subsets, such as regulatory T cells, PMN-MDSC, and E-MDSC, as well as exhausted T cells and NK cells, were found in the PDX from humanized mice. This is reflective of subpopulations that have appeared in the NPC microenvironment from paired archival tissue of the donor patients and in patients from other study (*43*). Besides, it has been proposed that localized immune responses in the TME cannot exist without continuous coordination with the peripheral immune system (*44*). In addition to the presence of humanized immune cells, various inflammatory cytokines (IFN-γ, IL-8, and IL-18), chemokine (MCP-1), and immune checkpoint biomarkers (Gal-9, sPD-L1, sCD25, and TGF-β1) were found in the circulation in PDX-bearing humanized mice. These peripheral immune cells and soluble mediators play a crucial role in tumor development, while these elements were either absent or minimally detected in the immunocompromised NSG mice. Because the coordination of the peripheral immune system and TME more closely resembles that in patients, the humanized mouse model can improve our understanding of systemic immunity during tumor progression and provide a more accurate platform to develop and assess antitumor efficacy and safety of different treatment regimens, particularly immunotherapies.

In our study, we found that sPD-L1 was present in the circulation of NPC-PDX–bearing humanized mice, and the membrane-bound PD-L1 expression level in the PDX from humanized mice was significantly higher when compared to that from NSG mice, where tumor cells, nonimmune stromal cells, and a minor population of $CD45^+$ TIL expressed the PD-L1 on their cell surface. It is possible that the presence of IFN-γ in humanized mice induces the PD-L1 expression on the tumor cells (*45*), which serves as an excellent target for both cell-mediated therapy and ICI therapy. As a proof of concept, our third-generation stable CAR NK92 cell line that targets PD-L1 showed superior cytotoxicity and induced apoptosis in various human cancer cell lines that express the PD-L1, and the results are comparable to those aforementioned studies using high-affinity NK92 cells (*46*–*48*). Upon coculturing with the PD-L1–expressing cancer cells, the CAR NK92 cells showed augmented degranulation, as reflected by increasing their CD107a expression and releasing more IFN-γ. Besides, the CAR NK92 cells could suppress the growth of C666-1 cells in NSG mice. Moreover, PD-L1–expressing NPC-PDX established from different donors were transplanted into the NSG mice. From our results, it was found that the CAR NK92 cells could hinder the growth of these PDX more effectively when compared to WT NK92 cells, suggesting that the antitumor effect of the CAR NK92 cells was not PDX specific. Similarly, the CAR NK92 cells could exhibit growth inhibitory effects on lung cancer A549 cells and LAC-PDX that express the PD-L1. These results demonstrated that our CAR-NK cells are efficient in killing different solid cancer types, both in vitro and in vivo.

To date, NK92 is the only human NK cell line that has been approved for NK cell–mediated therapy in clinical trials (*36*). These cells were derived from a progressive non-Hodgkin's lymphoma

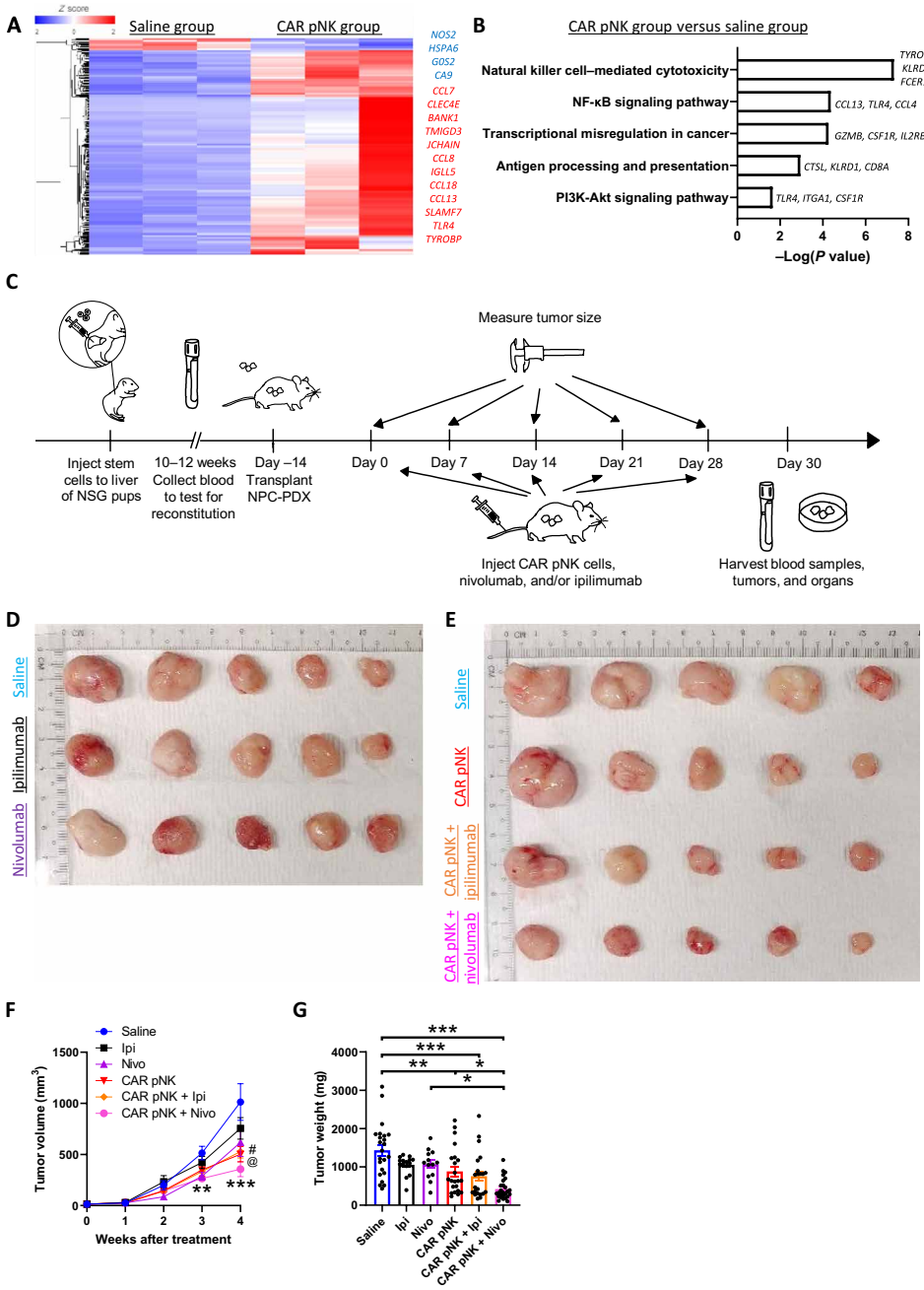

Fig. 7. Dual therapy using CAR pNK cells and nivolumab results in a synergistic antitumor response on NPC-PDX in humanized mice. (**A**) Heatmap of DE genes from NPC-PDX between CAR pNK cell–injected mice ($n = 3$) and saline-injected mice ($n = 3$) is shown. (**B**) Signaling pathway analysis of DE genes. (**C**) Schematic description of PDX engraftment, ICI therapy alone, or in combination with CAR pNK cell–mediated therapy in humanized mice. (**D** to **G**) Humanized mice were transplanted with NPC-PDX. After the formation of visible tumors, the mice were injected with saline ($n = 23$), ipilimumab ($n = 15$), nivolumab ($n = 13$), CAR pNK cells ($n = 22$), CAR pNK cells plus ipilimumab ($n = 22$), and CAR pNK cells plus nivolumab ($n = 26$). (D and E) Representative image of tumors. (F) Tumor volumes are shown. Data are expressed as means ± SEM. $^{**}P < 0.01$ and $^{***}P < 0.001$, when CAR pNK cells plus nivolumab–treated group is compared to saline-injected group, $@P < 0.05$, when CAR pNK cells plus ipilimumab–treated groups are compared to saline-injected group, $\#P < 0.05$, when CAR pNK cell–treated groups are compared to saline-injected group, one-way ANOVA followed by multiple comparisons. (G) Tumor weights are shown. Data are combined from at least three independent experiments using PDX derived from three patients and expressed as means ± SEM. $^{*}P < 0.05$, $^{**}P < 0.01$, and $^{***}P < 0.001$, one-way ANOVA followed by multiple comparisons.

(*49*), and irradiation of these cells is essential to reduce their proliferative ability before infusing them into patients (*36*). Apart from the NK92 cells, primary NK cells from human peripheral blood or cord blood can be isolated and genetically engineered with CAR for subsequent cell therapy. However, one of the major caveats is that the primary NK cells are resistant to gene transfer, where vesicular stomatitis virus type G lentiviral vectors that are typically used to generate CAR-T cells, calcium phosphate precipitation, liposome

reagents, and electroporation techniques showed a limited gene transduction rate (*50*). Until more recently, baboon envelope pseudotyped lentiviral vectors have been shown to improve the transduction efficiency (*51*). Alternatively, primary NK cells can be differentiated from multipotent progenitor cells and pluripotent stem cells, such as hESCs, iPSCs, mobilized bone marrow stem cells, and umbilical cord blood stem cells (*17*, *39*). Compared to mature NK cells, these progenitor and stem cells demonstrated higher transduction efficiency (*52*). In the current study, HSC obtained from human cord blood samples and differentiated into NK cells presents a viable method to develop CAR-NK cells for clinical use. We first illustrated that pNK cells showed similar phenotypes and functions when compared to CB-NK cells, despite the latter expressing a higher level of CD16. In clinic, large numbers of CAR-NK cells, ranging from 2×10^5 to 4×10^9 cells/kg, are needed for single or multiple infusions into patients (*52*, *53*). Compared to the CB-NK cells, HSC showed a better expansion capacity and transduction efficiency. Hence, it is feasible to generate an ample number of CAR pNK cells for single or multiple adoptive transfers. Apart from the cytotoxicity on PD-L1–expressing human cancer cell lines, the CAR pNK cells, but not CAR pT cells, could inhibit the growth of NPC-PDX in NSG mice. Despite there was a higher number of tumor-infiltrating CAR pT cells, the CAR pNK cell–mediated therapy could elicit more apoptosis in the tumors. One of the possibilities is that the NK cells can lyse tumor cells without prior priming, while the T cell function is major histocompatibility complex (MHC)–restricted (*54*). Further, we showed that our current CAR pNK cell–mediated therapy retained its antitumor potency on NPC-PDX despite the presence of tumor-infiltrating immunosuppressive leukocytes and the influence of TME in humanized mice. Accompanied by an increase in IFN-γ after cell-mediated therapy, the level of plasma sPD-L1 and membrane-bound PD-L1 expression in the PDX was enhanced, particularly in the mice treated with CAR pT cells. However, there were no significant changes in the tumor burden after the injection of CAR pT cells, suggesting that other factors, such as the release of soluble mediators upon binding to the PD-L1–expressing tumor cells, might affect their antitumor potency. Minimal CAR pNK cells and CAR pT cells persisted in the PDX 2 days after the last injection. It has been reported that CAR-NK cells generally had a short life span in vivo (*55*), while a hypoxia TME might disturb the cytotoxicity of NK cells and the recruitment of $CD8^+$ T cells into tumor areas (*56*, *57*). Further improvements of CAR design might be beneficial to the infiltration, cytotoxicity, and persistence of the CAR-expressing immune cells for better antitumor outcomes.

Administration of ICI targeting PD-1 and other immune checkpoints is now an established clinical treatment standard for NPC, as several exhausted and immunosuppressive cell subsets, including $HAVCR2^+PD\text{-}1^+$ T cells, $CD25^+FOXP3^+CTLA\text{-}4^+$ regulatory T cells, and $CD68^+$ myeloid-derived cells, are found in patient TME (*31*, *43*). However, the reported objective response rates using anti–PD-1 monoclonal antibody and other ICI were around 20% in different single-arm trials (*23*). Consistent with the lack of response in donor patients in the clinic, treatments involving ipilimumab or nivolumab alone did not reduce the burden of NPC-PDX in humanized mice, although more $CD3^+$ T cells were infiltrated into the PDX after ipilimumab treatment and CD4/CD8 ratio was reduced after nivolumab treatment when compared to saline-treated group. As demonstrated by our previous findings, the ICI treatment mainly restored the function of tumor-infiltrating T cells, which was indicated by an increase in their activation marker HLA-DR and cytokine production (*22*). However, the restoration of T cell function alone was not sufficient to reduce the tumor burden. In recent years, it has been proposed that other modes of cancer therapy, including radiotherapy, chemotherapy, and gene-targeted therapies, could modulate the immunosuppressive TME and potentially synergize with ICI therapy (*58*). Our RNA sequencing data revealed an increment in antigen processing and presentation pathway after the injection of CAR pNK cells in humanized mice, suggesting that the host immune system was also stimulated after the treatment, despite the existence of immunosuppressive and exhausted tumor-infiltrating immune cells. Thus, blocking inhibitory signals in these cells, in combination with the NK cell–mediated therapy, might further improve their antitumor functions. Encouragingly, treatment regimens involving CAR pNK cells and nivolumab, but not ipilimumab, resulted in a synergistic antitumor response in the humanized mice. It is anticipated that PD-L1–expressing tumor cells were first targeted and lysed by the CAR pNK cells, and the presented antigens were further recognized by tumor-infiltrating T cells to regress local tumors, where these cells could respond to specific ICI and reinvigorate their functions in our model. Further examinations of mRNA differential expression in NPC-PDX among different treatment regimens, such as CAR pNK cell–treated group, nivolumab-treated group, and CAR pNK cell and nivolumab-treated group, either in synchronous or sequential manner, might provide insights to identify potential therapeutic targets in the future, and the sequential administration of CAR pNK cells and nivolumab might result in different antitumor efficacy. Notably, the CAR pNK cells might acquire PD-1–expressing exhaustion phenotype when they infiltrated into the tumors, but considering the strong activation motifs carried by the CAR pNK cells and their short life span, the nivolumab treatment might not have remarkable impact on the tumor-infiltrating CAR pNK cells when compared to the host tumor-infiltrating T cells.

Apart from antitumor efficacy, the safety of NK cell–mediated therapy was investigated. After treatment with IFN-γ, there was an increase in PD-L1 expression on both PHH and HepG2 cell surface. However, CAR pNK cells showed limited in vitro cytotoxicity on the former, whereas the latter were more susceptible to the CAR pNK cells. Similarly, the CAR pNK cells exhibited minimal cytotoxicity on the $CD45^+$ TIL when compared to the tumor cells isolated from the same PDX. One of the possibilities is that NK cells recognize the absence of self-antigens on tumor cells via the interaction between killer cell Ig-like receptors on NK cell surface and MHC-I molecules on cancer cell surface. In contrast, normal healthy cells express MHC-I molecules on their surface, which serve as ligands for inhibitory receptors on NK cells and contribute to NK cell tolerance (*53*). Tumor-bearing humanized mice injected with CAR pT cells resulted in a drastic reduction in their survivability, when compared to that after CAR pNK treatment. It is conceivable that one of the side effects of T cell–mediated therapy is the induction of CRS, which is featured by a massive release of inflammatory cytokines, including IFN-γ, tumor necrosis factor–α, IL-6, and IL-10 (*11*, *59*). Consistently, we found that plasma concentrations of IFN-γ, IL-6, and IL-10 were significantly up-regulated in tumor-bearing humanized mice after CAR pT treatment but not in the CAR pNK cell–treated mice. In particular, the increase in IFN-γ might further induce the expression of mouse PD-L1 in liver and lung. Pathological conditions were observed in these organs, which might partially explain the reduction in mouse body weight and survivability after the CAR pT cell–mediated therapy. Notably, it has been suggested that host

immune cells play a crucial role in the pathogenesis of CRS, and depletion of macrophages and monocytes might reduce the severity of the CRS (*11*). Hence, further use of the humanized mouse model is warranted to identify mechanisms that lead to CRS and other irAE and to assess the safety of different cancer treatments, including but not limiting to cell-mediated therapy and ICI therapy.

Together, we illustrated that TME in the humanized mouse model more closely resembles that in patients. This provides a better platform to identify molecular targets, develop therapeutic drugs, and assess their antitumor efficacy and immunotoxicity in the presence of the humanized immune system. Pursuing an unmet need in the treatment of solid cancers, dual therapy using HSC-derived CAR pNK cells and nivolumab was tested in this study, and we observed a notable growth inhibitory effect on NPC-PDX in humanized mice. Besides, the expression levels of other immune checkpoint receptors, including but not limiting to TIGIT and TIM-3, were also up-regulated in the tumor-infiltrating T cells and NK cells in humanized mice, and their signaling is strongly associated with immune-response regulation and tumor progression (*60*). Hence, further evaluations of combination regimens in the humanized mice are highly warranted to provide insights for developing next-generation cancer immunotherapies and improve clinical outcomes in patients.

MATERIALS AND METHODS

Study design

TIL play a crucial role to shape TME and influence clinical outcomes of cancer treatments. In the presence of a humanized immune system, our model better simulates the TME in patients when compared to immunocompromised NSG mice. Hence, this study aimed to identify and validate potential targets for solid cancer treatments based on the TME difference between NSG mice and humanized mice. Taken as an example, we observe that membrane-bound PD-L1 was highly expressed in the PDX in humanized mice, thus serving as an excellent target for immune cell therapy. Hence, we established a CAR NK92 cell line targeting the PD-L1 to investigate in vitro and in vivo CAR-NK cell–mediated anti-solid tumor effects and the action mechanisms, if any. To minimize potential safety concern using the NK92 cell line, we further generated HSC-derived CAR pNK cells. The in vitro cytotoxicity of CAR pNK cells toward human cancer cells, in vivo anti-solid tumor efficacy and safety, action mechanisms, and transcriptomic changes were assessed. Notably, the immunosuppressive TME in humanized mice might lead to immune effector cells exhaustion, which hamper their antitumor functions. Hence, the anti-solid tumor efficacy of CAR pNK cells, either alone or in combination with different ICI, was evaluated. In our study, mice were randomly divided into different treatment groups once they showed tumor growth, and no animals were excluded because of humane end point. Researchers were not blinded to the treatments.

Mouse strain and generation of humanized mice

NSG mice were purchased from The Jackson Laboratory and bred in a specific pathogen–free condition at Biological Resource Centre in Agency for Science, Technology and Research (A*STAR), Singapore. Humanized mice were generated as described elsewhere (*22*). Briefly, human cord blood $CD34^+$ HSC (2×10^5 per pup; Lonza Bioscience, Basel, Switzerland) were inoculated into NSG pups by intrahepatic injection after the pups were sublethally irradiated at 1 Gy. Ten to 12 weeks after the injection, blood samples were collected from the mice, and human immune cell engraftment (chimerism) in the mice was determined by flow cytometry. The chimerism was calculated by [% human $CD45^+$/(% human $CD45^+$ + % mouse $CD45^+$)], and humanized mice with the chimerism between 20 and 50% were used for subsequent experiments.

SingHealth and National Health Care Group Research Ethics Committees Singapore specifically approved this study [Institutional Review Board (IRB) number: 2020-040]. All animal experiments were conducted in strict accordance with the guidelines on Care and Use of Animals for Scientific Purposes, which are released by the National Advisory Committee on Laboratory Animal Research, Agri-Food and Veterinary Authority of Singapore, and International Animal Care and Use Committee (IACUC) at A*STAR. The IACUC specifically approved this study (IACUC numbers: 181367 and 191440).

Nasopharyngeal carcinoma and LAC xenografts

Primary tumors of NPC and LAC were collected from National Cancer Center Singapore (NCCS), with written consent obtained from patients and in strict accordance with the institutional ethical guidelines of NCCS. SingHealth and National Health Care Group Research Ethics Committees Singapore specifically approved this study (IRB numbers: 2016/2887 and 2007/444/B). NPC-PDX and LAC-PDX were established in NSG mice as described previously (*22*).

RNA sequencing and data analysis

NPC-PDX in NSG mice and humanized mice were harvested, and total RNA was extracted using TRIzol Reagent (Thermo Fisher Scientific, Waltham, MA, USA). The total RNA of each sample was then quantified and qualified by NanoDrop (Thermo Fisher Scientific) and Agilent 2100 Bioanalyzer (Agilent Technologies, Palo Alto, CA, USA). Next, 1 μg of total RNA was used for library preparations according to the manufacturer's protocol (VAHTS mRNA-seq V3 Library Prep Kit for Illumina). The poly(A) mRNA isolation was performed using the Poly(A) mRNA Magnetic Isolation Module. The mRNA fragmentation and priming were performed using First-Strand Synthesis Reaction Buffer and Random Primers, where first- and second-strand cDNAs were synthesized using ProtoScript II Reverse Transcriptase and Second Strand Synthesis Enzyme Mix, respectively. The double-stranded cDNA was purified by beads and further treated with End Prep Enzyme Mix. Size selection of adaptor-ligated DNA was then performed using beads, and fragments of ~400 bp (with an approximate insert size of 300 bp) were recovered. The samples were amplified by polymerase chain reaction (PCR) using P5 and P7 primers. Subsequently, PCR products were cleaned up using beads, validated using a Qsep100 (Bioptic, Taiwan), and quantified by a Qubit 3.0 Fluorometer (Invitrogen, Carlsbad, CA, USA). Libraries with different indices were multiplexed and loaded on an Illumina Novaseq instrument according to the manufacturer's instructions (Illumina, San Diego, CA, USA). Sequencing was performed using a 2×150 paired-end configuration. Image analysis and base calling were conducted by NovaSeq Control Software + OLB + GAPipeline-1.6 (Illumina) on the NovaSeq instrument. After sequencing, the reads were analyzed on Partek Flow software (Partek Inc., St. Louis, MO, USA). In essence, the reads were mapped to the hg38 reference genome using STAR aligner. The aligned reads were quantified and annotated based on RefSeq transcripts (version 99). Differential gene expression analysis was performed using the Partek GSA algorithm, and overrepresentation enrichment analysis was performed using Kyoto Encyclopedia of Genes and Genomes Pathways (*Homo sapiens*).

Flow cytometric analysis

Before surface marker staining, all cells were stained with a dye provided in the LIVE/DEAD Fixable Blue Dead Cell Stain Kit (Sigma-Aldrich, Saint Louis, MO, USA) at room temperature for 15 min. To examine the presence of CAR on NK cell surface, biotinylated protein L (GeneScript, Piscataway, NJ, USA) and Allophycocyanin (APC)–conjugated streptavidin (BioLegend, San Diego, CA, USA) were used. In essence, the cells were stained with the biotinylated protein L (10 μg/ml) at 4°C for 15 min. Afterward, the cells were washed with phosphate-buffered saline (PBS) and incubated with the APC-conjugated streptavidin (5 μg/ml) at 4°C for 30 min.

To determine the binding between mouse PD-L1 recombinant protein and CAR on NK cell surface, the cells were incubated with mouse PD-L1 protein-His tag (10 μg/ml; Sino Biological Inc., China) at room temperature for 1 hour, followed by an incubation of APC-conjugated anti-His tag (R&D Systems, Minneapolis, MN, USA) at 4°C for 30 min.

The expression level of human PD-L1 on different cells was examined using anti-human PD-L1 (clone 29E.2A3) and isotype control antibodies (mouse IgG2b, clone MG2b-57). All FACS antibodies are purchased from BioLegend, unless otherwise specified. The following antibodies were used in this study: (i) anti-human antibodies: CD3 (clone UCHT1, BD Biosciences, Franklin Lakes, NJ, USA), CD4 (clone SK3, BD Biosciences), CD8 (clone SK1), CD11b (clone ICRF44), CD14 (clone HCD14), CD15 (clone W6D3), CD16 (clone 3G8), CD19 (clone HIB19), CD25 (clone 2A3, BD Biosciences), CD33 (clone WM53, BD Biosciences), CD34 (clone 581), CD45 (clone HI30, BD Biosciences), CD56 (clone HCD56), CD57 (clone QA17A04), CD94 (clone 18d3), CD107a (clone H4A3), CD127 (clone A019D5), CD133/2 (clone 293C3, Miltenyi Biotec, Germany), BTLA (clone MIH16), CTLA-4 (clone BNI3), HLA-DR (clone L243, BD Biosciences), LAG-3 (clone 3DS223H, Thermo Fisher Scientific), NKG2A (clone REA110, Miltenyi Biotec), NKG2D (clone REA797, Miltenyi Biotec), NKp30 (clone REA823, Miltenyi Biotec), NKp44 (clone 2.29, Miltenyi Biotec), NKp46 (clone 9E2/NKp46, BD Biosciences), PD-1 (clone EH12.1, BD Biosciences), TIGIT (clone MBSA43, Thermo Fisher Scientific), and TIM-3 (clone F38-2E2); (ii) anti-mouse antibody: CD45 (clone A20); (iii) isotype control antibodies: mouse G1 (MOPC-21) and rat IgG2a (clone RTK2758).

Flow cytometric analysis was performed on a LSRII flow cytometer using FACSDiva software (Becton Dickinson, Sparks, MD, USA). Hundred thousand events were collected per sample and analyzed using FlowJo software version 10 (TreeStar, Ashland, OR, USA).

Cytokine array

The relative protein expressions of intratumoral cytokines from NSG and humanized mice were analyzed using the Proteome Profiler Human Cytokine Array Kit (R&D Systems) according to the manufacturer's instructions. Briefly, NPC-PDX were harvested and tumor fragments were digested in radioimmunoprecipitation assay buffer (Thermo Fisher Scientific). Protein concentration was determined by Bio-Rad Protein Assay Dye Reagent Concentrate (Bio-Rad Laboratories, Hercules, CA, USA), and 200 μg of protein was applied to each membrane. The cytokines were detected using streptavidin–horseradish peroxidase and chemiluminescent reagent mix. Subsequently, the pixel density of each dot was determined using ImageJ software (National Institutes of Health, Bethesda, MD, USA), and the readout from each sample dot was normalized using the average reading of six positive control dots.

Quantification of plasma cytokines, chemokines, and immune checkpoint molecules

Plasma cytokines and chemokines levels and immune checkpoint biomarkers from NSG and humanized mice were determined by LEGENDplex Human CD8/NK Panel, Human Inflammation Panel 1, and HU Immune Checkpoint Panel 1 (BioLegend) according to the manufacturer's instructions. The profile was analyzed by flow cytometry and LEGENDplex data analysis software (BioLegend).

Quantitative real-time PCR

NPC-PDX in NSG mice and humanized mice were harvested. Tumors were first digested into single-cell suspension using the Tumor Dissociation Kit, Human (Miltenyi Biotec). Viable human cells in the cell suspensions were then selected using the Dead Cell Removal Kit (Miltenyi Biotec) and the Mouse Cell Depletion Kit (Miltenyi Biotec), followed by incubating with CD45 (TIL) MicroBeads, Human (Miltenyi Biotec). The eluted tumor cells were collected. Total RNA from the tumor cells was extracted using TRIzol Reagent and subjected to reverse transcription using the QuantiTect Reverse Transcription Kit (Qiagen, Germany). Gene expressions of human PD-L1 and human IFN-γ were quantified by real-time PCR using SsoFast EvaGreen supermix (Bio-Rad Laboratories). The reaction was performed on CFX Connect Real-Time PCR Detection System (Bio-Rad Laboratories). Relative gene expressions of the human PD-L1 and human IFN-γ were analyzed using the $2^{(-\Delta\Delta Ct)}$ method and normalized relative to human β-actin. Primer sequences used are listed as follows: human PD-L1 forward, 5′-GCTGCACTAATTGTCTATTGGGA-3′; human PD-L1 reverse, 5′-AATTCGCTTGTAGTCGGCACC-3′; human IFN-γ forward, 5′-TCGGTAACTGACTTGAATGTCCA-3′; human IFN-γ reverse, 5′-TCGCTTCCCTGTTTTAGCTGC-3′; human β-actin forward, 5′-GGGTCAGAAGGATTCCTATG-3′; human β-actin reverse, 5′-GGTCTCAAACATGATCTGGG-3′.

Similarly, total RNA from liver and lung from PDX-bearing humanized mice was extracted using TRIzol Reagent and subjected to reverse transcription using the QuantiTect Reverse Transcription Kit. Gene expression of mouse PD-L1 was quantified by real-time PCR, and relative gene expression of the mouse PD-L1 was analyzed as described above. Primer sequences used are listed as follows: mouse PD-L1 forward, 5′-GCTCCAAAGGACTTGTACGTG-3′; mouse PD-L1 reverse, 5′-TGATCTGAAGGGCAGCATTTC-3′; mouse β-actin forward, 5′-ACAGAGCCTCGCCTTTGCC-3′; mouse β-actin reverse, 5′-GATATCATCATCCATGGTGAGCTGG-3′.

Immunohistochemical staining

Tumors were formalin-fixed (Sigma-Aldrich) at room temperature for 24 hours, paraffin-embedded (Leica, Germany), sliced into 5-μm sections, and stained for human PD-L1, human CD3, and human NCR1 using their respective antibodies purchased from Abcam (Cambridge, MA, USA), followed by hematoxylin counterstain (Thermo Fisher Scientific). The stained images were captured using a ZEN fluorescence microscope (Zeiss, Germany) with ZEN 2 acquisition software (Zen Blue Version, Zeiss).

Immunofluorescence staining

Tumors were embedded and frozen. Fixed cryostat sections were incubated with anti-human CD3 antibody conjugated with Phycoerythrin (PE) (Miltenyi Biotec), anti-human CD45 antibody conjugated with PE (Miltenyi Biotec), anti-human CD56 antibody conjugated with PE (Miltenyi Biotec), and/or unconjugated anti-human PD-L1

antibody. After washing, slides were probed with Alexa Fluor 488 dye–conjugated secondary antibodies (Thermo Fisher Scientific), whenever indicated, mounted with ProLong Diamond Antifade Mountant (Thermo Fisher Scientific), and the signals were examined using an Eclipse Ti-E fluorescence microscope (Nikon, Tokyo, Japan).

To confirm successful transduction of CAR in NK92 cells, non-transduced WT NK92 and CAR NK92 cells (1×10^4 cells in 100 μl of PBS) were seeded onto a microscopic slide by cytocentrifugation at 500 rpm for 5 min using Shandon Cytospin centrifuge (Shandon Scientific Ltd., UK). The cells were then air-dried, fixed with 4% paraformaldehyde for 15 min, and mounted with ProLong Diamond Antifade Mountant. GFP signal in the cells was examined using an Eclipse Ti-E fluorescence microscope.

Cell culture

Human non-Hodgkin's lymphoma NK92 cells were cultured in complete RPMI 1640 medium (Cytiva Life Sciences, Marlborough, MA, USA) containing human IL-2 recombinant protein (200 IU/ml; Miltenyi Biotec) and 10% fetal bovine serum (FBS; Gibco, Grand Island, NY, USA). Human hepatocellular carcinoma HepG2 cells, human embryonic kidney (HEK) 293T cells, and lung carcinoma A549 cells were cultured in complete Dulbecco's modified Eagle's medium (Cytiva Life Sciences) containing 10% FBS. Human IFN-γ (Miltenyi Biotec) was supplemented at a concentration of 10 μg/ml medium, whenever indicated, to induce the expression of PD-L1 on the HepG2 cells or PHH. Human NPC C666-1 cells, erythroleukemic K-562 cells, and pancreatic carcinoma Panc 08.13 cells were cultured in complete RPMI 1640 medium containing 10% FBS. All the cell lines were purchased from American Type Culture Collection.

Primary NK cells were differentiated from human $CD34^+$ HSC using the StemSpan NK Cell Generation Kit according to the manufacturer's instructions (STEMCELL Technologies). The purity and phenotype of the cells were examined by flow cytometry after 28-day differentiation (fig. S8B). Human sPD-L1 recombinant protein (Thermo Fisher Scientific) was supplemented at a concentration of 500 pg/ml medium, whenever indicated, to treat the primary NK cells.

Primary T cells isolated from cord blood (Lonza Biosciences) were seeded in a 24-well plate and maintained in TexMACS medium (Miltenyi Biotec) supplemented with human IL-2 (20 IU/ml). Human sPD-L1 recombinant protein (500 pg/ml medium) and/or T cell TransAct (20 μl/ml medium; Miltenyi Biotec) was supplemented at a concentration of 500 pg/ml medium, whenever indicated, to treat the primary T cells. All the cell lines and primary cells were incubated in a humidified incubator containing 5% CO_2 at 37°C and passaged, whenever necessary, using aseptic technique.

Design of CAR construct and lentiviral transduction

The construct consisted of a ScFv domain, which targeted PD-L1, two costimulatory domains (CD28 and 4-1BB), and a CD3ζ activation domain. Lentivirus was obtained from the supernatant of HEK293T cells, followed by cotransfection of the CAR construct and third-generation viral packaging plasmids using Lipofectamine 3000 (Life Technologies, Carlsbad, CA, USA).

To transduce NK92 cells, 5×10^5 cells [in 400 μl of RPMI 1640, supplemented with polybrene (8 μg/ml)] were seeded in a 24-well plate, and 100 μl of viral supernatant was added. The plate was centrifuged at 2000*g* at 32°C for 2 hours, and the cells were incubated in a humidified incubator containing 5% CO_2 at 37°C. Puromycin (10 μg/ml; Gibco) was added to the NK92 cells after 3 days of transduction to establish a stable CAR-expressing NK92 cell line. For the generation of CAR-expressing primary NK cells, differentiated NK cells were transduced similar to NK92. To transduce primary T cells, the cells were seeded in a 24-well plate and activated in TexMACS medium containing T cell TransAct (20 μl/ml) and human IL-2 (20 IU/ml) according to the manufacturer's instructions. Two days after activation, lentiviral particle (100 μl) and polybrene (8 μg/ml) were added to the cells, and the plate was centrifuged at 2000*g* at 32°C for 2 hours. The cells were harvested for downstream applications 3 days after transduction. The expression of CAR was verified by flow cytometry before each experiment.

Cell lysis assay

To determine NK cell cytotoxicity on their target cells, CytoTox 96 Non-Radioactive Cytotoxicity Assay (Promega, Madison, WI, USA) was performed according to the manufacturer's instructions. Briefly, NK92 cells or primary NK cells (effector cells) were cocultured with HepG2, A549, C666-1, K-562, and Panc 08.13, isolated cells from NPC-PDX and PHH (target cells) at the indicated effector cell to target cell ratio (E:T) ratio at 37°C for 4 hours. After incubation, 50 μl of the cell-free supernatant was incubated with 50 μl of substrate solution at room temperature for 30 min, followed by the addition of stop solution. The absorbance at 490 nm was measured using an Infinite M200 plate reader (Tecan, Switzerland). The percentage of cytotoxicity was calculated using the following formula: % cytotoxicity = 100 × (corrected reading from test well − corrected reading from untreated well)/(corrected maximum release of lactate dehydrogenase control).

Measurement of DNA fragmentation

The induction of apoptosis was determined using the Cell Death Detection ELISAPLUS Kit (Sigma-Aldrich), and the experiments were conducted according to the manufacturer's instructions. NK92 cells or primary NK cells (5×10^5/ml) were cocultured with HepG2, A549, C666-1, K-562, and Panc 08.13 cells and isolated tumor cells from NPC-PDX (5×10^5/ml) in a flat-bottomed 96-well plate at 37°C for 4 hours. The cell-free supernatant was transferred to a streptavidin-coated 96-well microtiter plate, and the absorbance at 405 nm was recorded by an Infinite M200 plate reader. The degree of apoptosis was expressed as an enrichment factor, which was calculated as follows: Enrichment factor = Absorbance of the well with CAR-NK cells and cancer cells/absorbance of the well with WT-NK cells and cancer cells.

CD107a expression on NK cells and ELISA for human IFN-γ

NK92 cells or primary NK cells (5×10^5/ml) were cocultured with HepG2, A549, C666-1, K-562, and Panc 08.13 cells and isolated tumor cells from NPC-PDX (5×10^5/ml) in a flat-bottomed 96-well plate at 37°C for 4 hours. After incubation, the cells and the supernatant were collected to examine the expression level of CD107a on the NK cells and the release of IFN-γ, respectively. In short, the cells were stained with anti-human CD16, CD45, CD56, and CD107a antibodies at 4°C for 15 min before FACS analysis. The supernatant was centrifuged to remove cell debris, and the release of IFN-γ was quantified by ELISA MAX Deluxe Set Human IFN-γ (BioLegend) according to the manufacturer's instructions. The absorbance at 450 nm was recorded using an Infinite M200 plate reader.

In vivo NK cell–mediated therapy

To evaluate antitumor efficacy of cell-mediated therapy, 5×10^5 C666-1 cells or A549 cells, a piece of NPC-PDX or LAC-PDX (3 mm

by 3 mm fragment) was inoculated into the right flank of NSG mice and humanized mice. Once the tumor grew, 2.5×10^6 WT NK92, CAR NK92, WT pNK, CAR pNK, or CAR pT cells and nivolumab or ipilimumab (5 mg/kg mouse body weight) were injected intravenously into the mice every week for four consecutive weeks. Human IL-2 (1×10^4 IU per mouse) was administered together with the NK92 cells to promote NK cell survival and maintain their cytotoxicity, as described in an earlier study (*17*, *61*). Tumor measurement was performed weekly using a caliper as reported previously (*22*). Two days after the last injection, tumors were harvested and tumor weight was measured. Blood samples were collected in EDTA tubes (Greiner Bio-One, Monroe, NC, USA) through cardiac puncture.

TUNEL assay

Tumors were formalin-fixed, paraffin-embedded, and sliced as described above, and the presence of apoptotic cells was visualized using the In Situ Cell Death Detection Kit, TMR red (Sigma-Aldrich) according to the manufacturer's instructions. Briefly, tumor sections were dewaxed, rehydrated, and incubated with citrate buffer (pH 6) to achieve heat-induced epitope retrieval. After incubation, the sections were probed with the TUNEL reaction mixture at 4°C overnight. The slides were washed with PBS, mounted with ProLong Diamond Antifade Mountant, and imaged using an Eclipse Ti-E fluorescence microscope. The relative intensity of the signal was quantified with ImageJ software.

Hematoxylin and eosin staining

Liver and lungs from PDX-bearing humanized mice injected with saline, CAR pNK cells, or CAR pT cells were harvested 2 days after the last treatment. The samples were formalin-fixed, paraffin-embedded, sliced into 5-μm sections, and stained with hematoxylin and eosin (Thermo Fisher Scientific). Pathological evaluations were performed by an experienced research veterinary pathologist at the Advanced Molecular Pathology Laboratory from Institute of Molecular and Cell Biology (IMCB).

Statistical analysis

All statistical analyses were performed using GraphPad Prism version 9 (GraphPad Software Inc., La Jolla, CA, USA), and data are expressed as means ± SEs. Unpaired Student's *t* test, one-way analysis of variance (ANOVA) with post hoc Tukey's multiple comparisons test and two-way ANOVA were used, whenever appropriate, and Kaplan-Meier survival curves were analyzed by a log-rank test. The differences are considered statistically significant when $P < 0.05$.

SUPPLEMENTARY MATERIALS

Supplementary material for this article is available at https://science.org/doi/10.1126/sciadv.add1187

REFERENCES AND NOTES

1. C. Pucci, C. Martinelli, G. Ciofani, Innovative approaches for cancer treatment: Current perspectives and new challenges. *Ecancermedicalscience* **13**, 961 (2019).
2. J. Zugazagoitia, C. Guedes, S. Ponce, I. Ferrer, S. Molina-Pinelo, L. Paz-Ares, Current challenges in cancer treatment. *Clin. Ther.* **38**, 1551–1566 (2016).
3. X. Liu, G. D. Hogg, D. G. DeNardo, Rethinking immune checkpoint blockade: 'Beyond the T Cell'. *J. Immunother Cancer.* **9**, e001460 (2021).
4. Y. Lei, X. Li, Q. Huang, X. Zheng, M. Liu, Progress and challenges of predictive biomarkers for immune checkpoint blockade. *Front. Oncol.* **11**, 617335 (2021).
5. F. Martins, L. Sofiya, G. P. Sykiotis, F. Lamine, M. Maillard, M. Fraga, K. Shabafrouz, C. Ribi, A. Cairoli, Y. Guex-Crosier, T. Kuntzer, O. Michielin, S. Peters, G. Coukos, F. Spertini, J. A. Thompson, M. Obeid, Adverse effects of immune-checkpoint inhibitors: Epidemiology, management and surveillance. *Nat. Rev. Clin. Oncol.* **16**, 563–580 (2019).
6. M. Sadelain, I. Riviere, S. Riddell, Therapeutic T cell engineering. *Nature* **545**, 423–431 (2017).
7. C. H. June, R. S. O'Connor, O. U. Kawalekar, S. Ghassemi, M. C. Milone, Car T cell immunotherapy for human cancer. *Science* **359**, 1361–1365 (2018).
8. N. Albinger, J. Hartmann, E. Ullrich, Current status and perspective of car-T and Car-Nk cell therapy trials in Germany. *Gene Ther.* **28**, 513–527 (2021).
9. M. Themeli, I. Riviere, M. Sadelain, New cell sources for T cell engineering and adoptive immunotherapy. *Cell Stem Cell* **16**, 357–366 (2015).
10. J. N. Brudno, J. N. Kochenderfer, Recent advances in Car T-cell toxicity: Mechanisms, manifestations and management. *Blood Rev.* **34**, 45–55 (2019).
11. M. L. Schubert, M. Schmitt, L. Wang, C. A. Ramos, K. Jordan, C. Muller-Tidow, P. Dreger, Side-effect management of chimeric antigen receptor (Car) T-cell therapy. *Ann. Oncol.* **32**, 34–48 (2021).
12. E. Vivier, E. Tomasello, M. Baratin, T. Walzer, S. Ugolini, Functions of natural killer cells. *Nat. Immunol.* **9**, 503–510 (2008).
13. M. Zheng, R. Sun, H. Wei, Z. Tian, Nk cells help induce anti-hepatitis B virus Cd8+ T cell immunity in mice. *J. Immunol.* **196**, 4122–4131 (2016).
14. K. Rezvani, R. H. Rouce, The application of natural killer cell immunotherapy for the treatment of cancer. *Front. Immunol.* **6**, 578 (2015).
15. K. B. Lupo, S. Matosevic, Natural killer cells as allogeneic effectors in adoptive cancer immunotherapy. *Cancers* **11**, 769 (2019).
16. D. A. Knorr, A. Bock, R. J. Brentjens, D. S. Kaufman, Engineered human embryonic stem cell-derived lymphocytes to study in vivo trafficking and immunotherapy. *Stem Cells Dev.* **22**, 1861–1869 (2013).
17. Y. Li, D. L. Hermanson, B. S. Moriarity, D. S. Kaufman, Human Ipsc-derived natural killer cells engineered with chimeric antigen receptors enhance anti-tumor activity. *Cell Stem Cell.* **23**, 181–192.e5 (2018).
18. J. Bi, Z. Tian, NK cell exhaustion. *Front Immunol.* **8**, 760 (2017).
19. S. E. Franks, B. Wolfson, J. W. Hodge, Natural born killers: Nk cells in cancer therapy. *Cancers* **12**, 2131 (2020).
20. M. Binnewies, E. W. Roberts, K. Kersten, V. Chan, D. F. Fearon, M. Merad, L. M. Coussens, D. I. Gabrilovich, S. Ostrand-Rosenberg, C. C. Hedrick, R. H. Vonderheide, M. J. Pittet, R. K. Jain, W. Zou, T. K. Howcroft, E. C. Woodhouse, R. A. Weinberg, M. F. Krummel, Understanding the tumor immune microenvironment (Time) for effective therapy. *Nat. Med.* **24**, 541–550 (2018).
21. F. Petitprez, M. Meylan, A. de Reynies, C. Sautes-Fridman, W. H. Fridman, The tumor microenvironment in the response to immune checkpoint blockade therapies. *Front. Immunol.* **11**, 784 (2020).
22. W. N. Liu, S. Y. Fong, W. W. S. Tan, S. Y. Tan, M. Liu, J. Y. Cheng, S. Lim, L. Suteja, E. K. Huang, J. K. Y. Chan, N. G. Iyer, J. P. S. Yeong, D. W. Lim, Q. Chen, Establishment and characterization of humanized mouse Npc-Pdx model for testing immunotherapy. *Cancers (Basel).* **12**, 1025 (2020).
23. Y. P. Chen, A. T. C. Chan, Q. T. Le, P. Blanchard, Y. Sun, J. Ma, Nasopharyngeal carcinoma. *Lancet* **394**, 64–80 (2019).
24. L. Liu, Q. Zhao, C. Cheng, J. Yi, H. Sun, Q. Wang, W. Quan, Y. Xue, L. Sun, X. Cong, Y. Zhang, Analysis of bulk Rna sequencing data reveals novel transcription factors associated with immune infiltration among multiple cancers. *Front. Immunol.* **12**, 644350 (2021).
25. C. X. Li, C. C. Ling, Y. Shao, A. Xu, X. C. Li, K. T. Ng, X. B. Liu, Y. Y. Ma, X. Qi, H. Liu, J. Liu, O. W. Yeung, X. X. Yang, Q. S. Liu, Y. F. Lam, Y. Zhai, C. M. Lo, K. Man, Cxcl10/Cxcr3 signaling mobilized-regulatory T cells promote liver tumor recurrence after transplantation. *J. Hepatol.* **65**, 944–952 (2016).
26. S. Eikawa, Y. Ohue, K. Kitaoka, T. Aji, A. Uenaka, M. Oka, E. Nakayama, Enrichment of Foxp3+ Cd4 regulatory T cells in migrated T cells to Il-6- and Il-8-expressing tumors through predominant induction of Cxcr1 by Il-6. *J. Immunol.* **185**, 6734–6740 (2010).
27. H. Liu, C. C. Ling, W. H. O. Yeung, L. Pang, J. Liu, J. Zhou, W. Y. Zhang, X. B. Liu, T. P. K. Ng, X. X. Yang, C. M. Lo, K. Man, Monocytic Mdsc mobilization promotes tumor recurrence after liver transplantation via Cxcl10/Tlr4/Mmp14 signaling. *Cell Death Dis.* **12**, 489 (2021).
28. C. Alfaro, A. Teijeira, C. Onate, G. Perez, M. F. Sanmamed, M. P. Andueza, D. Alignani, S. Labiano, A. Azpilikueta, A. Rodriguez-Paulete, S. Garasa, J. P. Fusco, A. Aznar, S. Inoges, M. De Pizzol, M. Allegretti, J. Medina-Echeverz, P. Berraondo, J. L. Perez-Gracia, I. Melero, Tumor-produced interleukin-8 attracts human myeloid-derived suppressor cells and elicits extrusion of neutrophil extracellular traps (Nets). *Clin. Cancer Res.* **22**, 3924–3936 (2016).
29. M. H. Kubala, V. Punj, V. R. Placencio-Hickok, H. Fang, G. E. Fernandez, R. Sposto, Y. A. DeClerck, Plasminogen activator inhibitor-1 promotes the recruitment and polarization of macrophages in cancer. *Cell Rep.* **25**, 2177–2191.e7 (2018).
30. N. Karin, H. Razon, Chemokines beyond chemo-attraction: Cxcl10 and its significant role in cancer and autoimmunity. *Cytokine* **109**, 24–28 (2018).
31. L. Gong, D. L. Kwong, W. Dai, P. Wu, Y. Wang, A. W. Lee, X. Y. Guan, The stromal and immune landscape of nasopharyngeal carcinoma and its implications for precision medicine targeting the tumor microenvironment. *Front. Oncol.* **11**, 744889 (2021).

32. J. Wyss, B. Dislich, V. H. Koelzer, J. A. Galvan, H. Dawson, M. Hadrich, D. Inderbitzin, A. Lugli, I. Zlobec, M. D. Berger, Stromal Pd-1/Pd-L1 expression predicts outcome in colon cancer patients. *Clin. Colorectal Cancer* **18**, e20–e38 (2019).
33. B. Seliger, Basis of Pd1/Pd-L1 therapies. *J Clin Med.* **8**, 2168 (2019).
34. J. M. Kim, D. S. Chen, Immune escape to Pd-L1/Pd-1 blockade: Seven steps to success (or Failure). *Ann. Oncol.* **27**, 1492–1504 (2016).
35. C. S. Backes, K. S. Friedmann, S. Mang, A. Knorck, M. Hoth, C. Kummerow, Natural killer cells induce distinct modes of cancer cell death: Discrimination, quantification, and modulation of apoptosis, necrosis, and mixed forms. *J. Biol. Chem.* **293**, 16348–16363 (2018).
36. H. Klingemann, L. Boissel, F. Toneguzzo, Natural killer cells for immunotherapy - Advantages of the Nk-92 cell line over blood Nk cells. *Front. Immunol.* **7**, 91 (2016).
37. C. Chabannon, B. Mfarrej, S. Guia, S. Ugolini, R. Devillier, D. Blaise, E. Vivier, B. Calmels, Manufacturing natural killer cells as medicinal products. *Front. Immunol.* **7**, 504 (2016).
38. D. A. Knorr, Z. Ni, D. Hermanson, M. K. Hexum, L. Bendzick, L. J. Cooper, D. A. Lee, D. S. Kaufman, Clinical-scale derivation of natural killer cells from human pluripotent stem cells for cancer therapy. *Stem Cells Transl. Med.* **2**, 274–283 (2013).
39. M. Luevano, A. Madrigal, A. Saudemont, Generation of natural killer cells from hematopoietic stem cells in vitro for immunotherapy. *Cell. Mol. Immunol.* **9**, 310–320 (2012).
40. K. Magiera-Mularz, J. Kocik, B. Musielak, J. Plewka, D. Sala, M. Machula, P. Grudnik, M. Hajduk, M. Czepiel, M. Siedlar, T. A. Holak, L. Skalniak, Human and mouse Pd-L1: Similar molecular structure, but different druggability profiles. *iScience* **24**, 101960 (2021).
41. Y. Zhao, J. Wang, W. N. Liu, S. Y. Fong, T. W. H. Shuen, M. Liu, S. Harden, S. Y. Tan, J. Y. Cheng, W. W. S. Tan, J. K. Y. Chan, C. E. Chee, G. H. Lee, H. C. Toh, S. G. Lim, Y. Wan, Q. Chen, Analysis and validation of human targets and treatments using a hepatocellular carcinoma-immune humanized mouse model. *Hepatology* **74**, 1395–1410 (2021).
42. Y. Zhao, T. W. H. Shuen, T. B. Toh, X. Y. Chan, M. Liu, S. Y. Tan, Y. Fan, H. Yang, S. G. Lyer, G. K. Bonney, E. Loh, K. T. E. Chang, T. C. Tan, W. Zhai, J. K. Y. Chan, E. K. Chow, C. E. Chee, G. H. Lee, Y. Y. Dan, P. K. Chow, H. C. Toh, S. G. Lim, Q. Chen, Development of a new patient-derived xenograft humanised mouse model to study human-specific tumour microenvironment and immunotherapy. *Gut* **67**, 1845–1854 (2018).
43. L. Gong, D. L. Kwong, W. Dai, P. Wu, S. Li, Q. Yan, Y. Zhang, B. Zhang, X. Fang, L. Liu, M. Luo, B. Liu, L. K. Chow, Q. Chen, J. Huang, V. H. Lee, K. O. Lam, A. W. Lo, Z. Chen, Y. Wang, A. W. Lee, X. Y. Guan, Comprehensive single-cell sequencing reveals the stromal dynamics and tumor-specific characteristics in the microenvironment of nasopharyngeal carcinoma. *Nat. Commun.* **12**, 1540 (2021).
44. K. J. Hiam-Galvez, B. M. Allen, M. H. Spitzer, Systemic immunity in cancer. *Nat. Rev. Cancer* **21**, 345–359 (2021).
45. W. Qin, L. Hu, X. Zhang, S. Jiang, J. Li, Z. Zhang, X. Wang, The diverse function of Pd-1/Pd-L pathway beyond cancer. *Front. Immunol.* **10**, 2298 (2019).
46. K. P. Fabian, M. R. Padget, R. N. Donahue, K. Solocinski, Y. Robbins, C. T. Allen, J. H. Lee, S. Rabizadeh, P. Soon-Shiong, J. Schlom, J. W. Hodge, Pd-L1 targeting high-affinity Nk (T-haNK) cells induce direct antitumor effects and target suppressive MDSC populations. *J. Immunother. Cancer.* **8**, e000450 (2020).
47. Y. Robbins, S. Greene, J. Friedman, P. E. Clavijo, C. Van Waes, K. P. Fabian, M. R. Padget, H. Abdul Sater, J. H. Lee, P. Soon-Shiong, J. Gulley, J. Schlom, J. W. Hodge, C. T. Allen, Tumor control via targeting Pd-L1 with chimeric antigen receptor modified Nk cells. *Elife* **9**, e54854 (2020).
48. M. Y. Lee, Y. Robbins, C. Sievers, J. Friedman, H. Abdul Sater, P. E. Clavijo, N. Judd, E. Tsong, C. Silvin, P. Soon-Shiong, M. R. Padget, J. Schlom, J. Hodge, C. Hinrichs, C. Allen, Chimeric antigen receptor engineered Nk cellular immunotherapy overcomes the selection of T-cell escape variant cancer cells. *J. Immunother. Cancer.* **9**, e002128 (2021).
49. J. H. Gong, G. Maki, H. G. Klingemann, Characterization of a human cell line (Nk-92) with phenotypical and functional characteristics of activated natural killer cells. *Leukemia* **8**, 652–658 (1994).
50. E. M. Grund, R. C. Muise-Helmericks, Cost efficient and effective gene transfer into the human natural killer cell line, Nk92. *J. Immunol. Methods* **296**, 31–36 (2005).
51. A. B. L. Colamartino, W. Lemieux, P. Bifsha, S. Nicoletti, N. Chakravarti, J. Sanz, H. Romero, S. Selleri, K. Beland, M. Guiot, C. Tremblay-Laganiere, R. Dicaire, L. Barreiro, D. A. Lee, E. Verhoeyen, E. Haddad, Efficient and robust Nk-cell transduction with baboon envelope pseudotyped lentivector. *Front. Immunol.* **10**, 2873 (2019).
52. S. Kundu, M. Gurney, M. O'Dwyer, Generating natural killer cells for adoptive transfer: Expanding horizons. *Cytotherapy* **23**, 559–566 (2021).
53. S. Oh, J. H. Lee, K. Kwack, S. W. Choi, Natural killer cell therapy: A new treatment paradigm for solid tumors. *Cancers* **11**, 1534 (2019).
54. R. V. Uzhachenko, A. Shanker, Cd8(+) T lymphocyte and Nk cell network: Circuitry in the cytotoxic domain of immunity. *Front. Immunol.* **10**, 1906 (2019).
55. M. Daher, L. Melo Garcia, Y. Li, K. Rezvani, Car-Nk cells: The next wave of cellular therapy for cancer. *Clin. Transl Immunology* **10**, e1274 (2021).
56. X. Zheng, Y. Qian, B. Fu, D. Jiao, Y. Jiang, P. Chen, Y. Shen, H. Zhang, R. Sun, Z. Tian, H. Wei, Mitochondrial fragmentation limits Nk cell-based tumor immunosurveillance. *Nat. Immunol.* **20**, 1656–1667 (2019).
57. P. Jayaprakash, M. Ai, A. Liu, P. Budhani, T. Bartkowiak, J. Sheng, C. Ager, C. Nicholas, A. R. Jaiswal, Y. Sun, K. Shah, S. Balasubramanyam, N. Li, G. Wang, J. Ning, A. Zal, T. Zal, M. A. Curran, Targeted hypoxia reduction restores T cell infiltration and sensitizes prostate cancer to immunotherapy. *J. Clin. Invest.* **128**, 5137–5149 (2018).
58. M. A. Postow, M. K. Callahan, J. D. Wolchok, Immune checkpoint blockade in cancer therapy. *J. Clin. Oncol.* **33**, 1974–1982 (2015).
59. A. Cortes-Hernández, E. K. Alvarez-Salazar, G. Soldevila, Chimeric antigen receptor (Car) T cell therapy for cancer. Challenges and opportunities: An overview. *Methods Mol. Biol.* **2174**, 219–244 (2021).
60. X. He, C. Xu, Immune checkpoint signaling and cancer immunotherapy. *Cell Res.* **30**, 660–669 (2020).
61. Y. K. Tam, G. Maki, B. Miyagawa, B. Hennemann, T. Tonn, H. G. Klingemann, Characterization of genetically altered, interleukin 2-independent natural killer cell lines suitable for adoptive cellular immunotherapy. *Hum. Gene Ther.* **10**, 1359–1373 (1999).

Acknowledgments

Funding: This work was supported by National Research Foundation Singapore Fellowship NRF-NRFF2017-03 (to Q.C.), A*STAR BMRC Central Research Fund (ATR) (to Q.C.), 2020 A*STAR Career Development Award 20701/C210112003 (to W.N.L.), NRF-ISF joint grant NRF2019-NRF-ISF003-3127 (to Q.C.), Industry Alignment Fund–Industry Collaboration Projects (IAF-ICP) Grant ICP-2000120 (to Q.C.), National Medical Research Council Clinician Scientist Individual Research Grant CIRG19may-0051 (to D.W.-T.L.), Industry Alignment Fund–Industry Pre-positioning Program (IAF-PP) Grant H18/01/a0/022 (to Q.C.), and National Medical Research Council-OF-LCG OFLCG19May-0038 (to Q.C.). **Author contributions:** Conceptualization: W.N.L. and Q.C. Methodology: W.N.L. and Q.C. Investigation: W.N.L., W.Y.S., S.L.H., S.Y.F., M.X.Y.W., W.W.S.T., S.Y.T., J.K.L.O., R.R., M.L., J.Y.C., L.S., and J.P.S.Y. Visualization: W.N.L. and J.K.L.O. Funding acquisition: W.N.L., D.W.-T.L., and Q.C. Project administration: N.G.I., D.W.-T.L., and Q.C. Supervision: D.W.-T.L. and Q.C. Writing—original draft: W.N.L. Writing—review and editing: W.N.L., W.Y.S., S.L.H., N.G.I., D.W.-T.L., and Q.C. **Competing interests:** Q.C. is the scientific founder of two biotech companies. The other authors declare that they have no competing interests. **Data and materials availability:** All data needed to evaluate the conclusions in the paper are present in the paper and/or the Supplementary Materials.

Submitted 21 May 2022
Accepted 5 October 2022
Published 23 November 2022
10.1126/sciadv.add1187